6-2014

Improved Accuracy in Real-Time RFID Localization Systems Using Kalman Filtering

Benjamin J. Sanda
Western Michigan University

IMPROVED ACCURACY IN REAL-TIME RFID LOCALIZATION SYSTEMS USING KALMAN FILTERING

by

Benjamin J. Sanda

A thesis submitted to the Graduate College
in partial fulfillment of the requirements
for the degree of Master of Science in Engineering
Electrical and Computer Engineering
Western Michigan University
June 2014

Thesis Committee:

Ikhlas Abdel-Qader, Ph.D., Chair
Bradley J. Bazuin, Ph.D.
Abiola A. Akanmu, Ph.D.

IMPROVED ACCURACY IN REAL-TIME RFID LOCALIZATION SYSTEMS USING KALMAN FILTERING

Benjamin J. Sanda, M.S.E.

Western Michigan University, 2014

The use of Radio Frequency Identification (RFID) has become widespread in industry as a means to quickly and wirelessly identify and track packages and equipment. Now there is a commercial interest in using RFID to provide real-time localization. Efforts to use RFID technology for this purpose experience localization errors due to noise and multipath effects inherent to these environments. This paper presents the use of both linear Kalman filters and non-linear Unscented Kalman filters to reduce error effects inherent to real-time RFID localization systems and provide more accurate localization results in indoor environments. A commercial RFID localization system designed for use by the construction industry is used in this work, and a filtering model based on 3rd order motion is developed. The filtering model is tested with real-world data and shown to provide an increase in localization accuracy when applied to both raw time of arrival measurements as well as final localization results.

ACKNOWLEDGMENTS

First I would like to thank Dr. Abiola Akanmu of the Civil and Construction Engineering Dept. at Western Michigan University for partnering with me and allowing the use of her lab and equipment. I would also like to thank her two former graduate students, Syed Hammad Rasheed and Bushra Asfari. Hammad developed the MySQL and Visual Studio code which allowed me to extract the CSL RTLS data samples for analysis, and Bushra assisted in setting up and acquiring data from the CSL RTLS. Thanks also to GR Makers, the Grand Rapids Makers Group, for supporting my work and allowing me use of their space for testing.

Thank you of course to my advisor and thesis committee chair Dr. Ikhlas Abdel-Qader who has guided and supported me on this journey, often with chocolate, and helped cement my desire to pursue further work in academia and teaching. I take her spirit and passionate joy of life and teaching with me. Also thanks to Dr. Bradley Bazuin, committee member and professor, who's seemingly encyclopedic knowledge of all things wireless and communication never ceases to amaze, and who forces me to read and research everything I can as I always know there is more.

Thanks to my engineering coworkers and friends who have supported me, always showed interest in my work, and allowed me to keep a horribly unpredictable schedule while working on this research. Particular thanks to my manger at Dornerworks, Matthew Remijn, and coworker Kathryn Hadley, for their steadfast support and uncompromising proofreading skills.

Without our history we would be nothing. Therefore I must thank two teachers, instructors, mentors, who helped guide my life and who's lessons have, and always will, serve me in good stead. To my first great teacher, Stanley Bidlack, who's exuberant soul, warm heart, and, shall we say, eccentric, teaching style has inspired me and shaped the teacher I

am today, and will continue to shape the teacher I am to be tomorrow. Second to the professor who helped make me the engineer I am today, Dr. Andrew Sterian, who's uncompromising pursuit of excellence, self discovery, and ingenuity have guided me in my professional and academic life and will continue to do so well into the future.

Finally, to my parental units, from whom I was spawned into this crazy and wonderful world. Thank you for putting up with a weird, rarely speaking, never normal, highly eccentric, never conforming to any norm or popular idea, truly unique child. Thank you for supporting me and allowing me grow up to be exactly who I am — not who anything or anyone wanted or thought I should be. Thank you for always being there, supporting me, and nurturing me, and for being there now to support me on this journey forward.

And remember, as a wise man once said, don't take any wooden nickels!

Benjamin J. Sanda

TABLE OF CONTENTS

LIST OF TABLES

LIST OF FIGURES

Chapter 1

Introduction

Indoor object localization and tracking is a growing field with direct applications in both the private and public sectors. The ability to track people and objects indoors, in real-time, is a valuable tool both for business and government. In the public sector localization can provide lifesaving information to military, law enforcement, and emergency services [1], as well as inform traffic and city management. In the construction industry object tracking is a growing field with important applications to asset and building site management [2].

GPS provides highly-accurate and functional localization outdoors but performs poorly indoors where direct line-of-sight to GPS satellites is not possible. As there is no direct means to allow GPS to function indoors, novel indoor localization systems must utilize a completely different methodology. Alternatives to GPS primarily utilize existing wireless systems and expand their functionality to include localization. Prominent methods include *IEEE 802.11* wireless LAN, ultrasonic and infrared methods, laser range finding, and Radio Frequency Identification (RFID) [3].

All of these methods however, suffer from noise and multipath interference. To combat this one option is the family of Kalman filters (KF). The KF is a predictive filtering model that can be applied to noisy systems to predict the actual system state based on recursive sampling. Used widely in GPS tracking, navigational guidance systems, and image detection, it is a powerful tool for noise reduction and system control. When applied to localization problems KF can reduce the effects of multipath and time of arrival (TOA) errors and increase the feasibility of these systems for real-world applications [4, 5].

Existing work has used mainly simulated data and statistical models and has lacked real-world experimentation. This paper presents the application of linear and non-linear

KF to a commercial TOA based RFID localization system operating in indoor environments. The RFID system is set up in an indoor environment containing noise and non-line of sight situations. Real-time data is collected, and KF techniques are designed based on the output and statistics of the system. The performance of the KF is analyzed and linear and non-linear implementations of the KF are also compared.

1 RFID Localization

RFID localization involves the use of multiple, long-range, RFID readers (antennas) set up in a known grid pattern to create a enclosed tracking area. Using the readers a system can track the location of a tag within the tracking area using either TOA and trilateration, time-difference of arrival (TDOA) and trilateration, or angle of arrival (AOA) and triangulation. Depending on the size and capabilities of the system just one, or multiple tags may be tracked simultaneously. Data is collected from the system via a data uplink from the readers to a control or monitoring PC. The PC generally provides software which performs analysis and graphical display of the tracking information. A typical system layout is shown in Figure 1.1.

As RFID localization utilizes TOA/TDOA/AOA methods of localization, it is very susceptible to noise, detuning, and multipath effects. These effects are especially intensified in indoor environments where there may be large metal obstacles and non-line of sight in the tracking area. The exact position of the readers must also be known and any error in reader location will propagate errors throughout the system.

There are three main types of RFID tags, some more useful to localization than others. The first and simplest type are passive RFID tags. These tags tend to be small, have no on-board power source of any kind, and operate in low frequency (LF), high frequency (HF), and ultra-high frequency (UHF) ranges. As the tags have no on-board power, they must utilize power harvesting techniques to capture or modify the power from the transmissions of the RFID readers. Because of their power constraints, passive tags also have a relatively short usable range of up to 3-10 feet and only maintain a static set of data.

LF and HF passive tags use inductive coupling to power a small microcontroller on

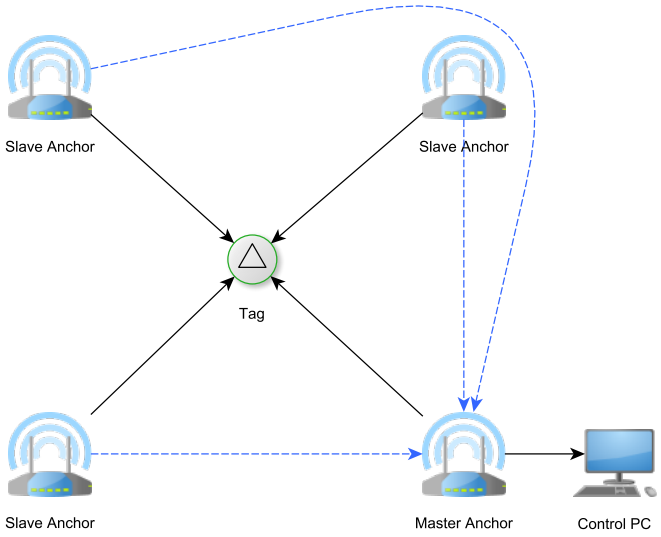

Figure 1.1: RFID localization system layout

board. The microcontroller then drives the transmit antenna and returns a signal to the receiver. Transmissions in the UHF range lack enough power to successfully use inductive coupling and so tags which operate in this range use a different technique called propagation coupling (backscatter). Instead of harvesting the transmission's power, they have a special antenna configuration which modulates the transmitted signal and reflects it back to the receiver. Based on the modulation the receiver can determine the information encoded on the tag.

The second type of RFID tag are active tags. These, as the name suggests, have on-board power sources and do not need to rely on power harvesting techniques as passive tags do. They tend to be larger then passive tags due to their power source, and also have much larger usable ranges then passive tags. Active tags may also support other on-board telemetry functions such as temperature, pressure, and light sensors, and have dynamic data sets. Active tags may operate in any of the defined RFID frequency ranges.

The third and final class of RFID tags are semi-passive tags. These are a hybrid tag which have on-board power, but only to power other on-board processing or telemetry functions, not to power the RFID transmitter. They have a similar read range as passive tags, but may support other telemetry or processing functions normal passive tags do not.

While passive tags are generally smaller, more robust, and cheaper, it is clear that for

any large scale tracking system active tags are the best option. They provide the range and enhanced signal strength needed to satisfy a large tracking area. The downsides of active tags are they are more expensive, less rugged, and require batteries or other power sources which must be monitored periodically replaced.

2 CSL Real-Time Localization System

The CSL Real-Time Localization System (CSL RTLS) is a commercial indoor/outdoor RFID-based tag localization system developed for use in construction and work site management [6]. The system identifies and tracks RFID tag location using a trilateration technique based on the TOA measurement calculated between a tag and at least two reference points (the system provides two-dimensional localization only). Using this data it maps and tracks all known tags and provides a PC-based interface for monitoring.

The system utilizes two main components: RFID tags and anchors. The RFID tags may be active or passive tags and are attached directly to objects of interest. These communicate with the anchors to provide ranging data as the object is positioned and moved within the tracking area. The anchors (readers) communicate with the tags to obtain TOA trilateration data as well as general tag information.

Two types of anchors are used by the system, slave anchors and master anchors. Slave anchors collect ranging data from the tags in their immediate area or cell. This data is then transmitted to the master anchor. The master anchor communicates with the slave anchors as well as serving as the gateway to the control PC. All slave anchors within a given area communicate with a single master anchor to transmit their ranging data to the control PC. There may be multiple master anchors depending on the size of the implementation site. The master anchor also serves as the controller for the system and manages the data collection rate among the slaves. If needed the master may also serve as a slave to collect ranging information from tags.

In this system, areas of the worksite are divided into cells, where each cell is managed by a given number of slave anchors and one master anchor. The maximum size of each cell is 200x200 m, and cells are generally sized and arranged logically based on the worksite

layout. As a tag moves from cell to cell the system automatically determines which slave anchors are best positioned to track the tag at any given time. When multiple cells and anchors are used, the system manages tag movement and cell communication using built-in roaming and jam avoidance schemes.

As a tag moves between adjacent cells the system implements a 2 m hysteresis to prevent unnecessary cell switching. The tag remains with the original cell until it has passed at least 2 m into the adjacent cell. Once the tag moves beyond this 2 m boundary into the adjacent cell the PC control software will handover tracking to the adjacent cell. To avoid communications conflicts the system uses time-division multiplexing. Adjacent cells use different time slots, and distant cells re-use time slots used by other distant cells if new slots are not available. This prevents nearby cells interfering with each other, and allows time slots to be re-used in the overall region.

At least three anchors are needed to perform the trilateration calculation, but the system supports up to eight per tracking area. The system determines which anchors to use by comparing the received signal strength indication (RSSI) between each anchor and the tag. The RSSI is an indication of the signal strength, and thus relative proximity and line-of-sight performance between the tag and an anchor. The tag-anchor pairs with the highest RSSI are then chosen by the system for use in the calculation.

Basic system performance metrics are given as follows [6]. Anchor requirements: 200x200 m cell requires at least 8 anchors. Outdoor accuracy: $\pm$ 1 m, indoor accuracy: $\pm$ 2 m. Number of slave anchors: 255 per cell (assuming 1 master anchor per cell). Number of tags: 65535 per cell. Operating frequency: 2400-2483 MHz ISM band.

2.1 Time of Arrival

TOA, also known as time-of-flight, is a method of localization which uses the distance between an emitter and three receivers to determine the location of the emitter. The distance between the emitter and tag is calculated by measuring the time the emitter's signal takes to reach each receiver. When three distances are known, they form three intersecting circles each with radius equal to the distance between the receiver and tag respectively as shown in Figure 1.2.

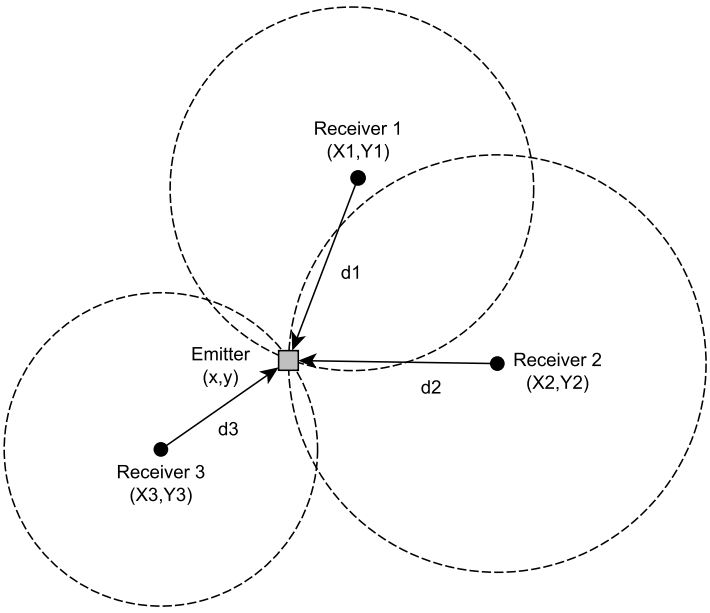

Figure 1.2: Time of arrival trilateration

Assuming three receivers with known locations, (X_i, Y_i), and emitter with position (x_t, y_t) [7]:

$$d_i = \sqrt{(X_i - x_t)^2 + (Y_i - y_t)^2} \tag{1.1}$$

Where d_i is the euclidean distance between the i-th receiver and the emitter. The distance, d_i, can be computed using the RSSI as:

$$\text{RSSI}_i = A - 10n_{Ai}\log(d_i) \tag{1.2}$$

$$d_i = 10^{-\frac{RSSI_i - A}{10n_{Ai}}} \tag{1.3}$$

Where A (dBm) and n_{Ai} (dBm) are propagation parameters unique to the radio frequency transmission. Alternately, the distance can also be computed using the time of arrival and the velocity of the radio wave as:

$$d_i = V_\tau t_i \tag{1.4}$$

Where t_i is time of arrival time from the emitter to the i-th receiver, and V_τ is the velocity of the radio wave (generally assumed to be equal to the speed of light, c).

3 Existing Work

There exists a large body of work concerning the application of the UKF and KF to tracking and localization scenarios. [8] describes the use of both the EKF and UKF to filter a simulated RFID tracking system. The tag positions were simulated using an RSSI propagation model and it was found the UKF outperformed the EKF. Similarly [9] applies the UKF to a simulated model of mail cart movement within a German mail processing center, Deutsche Post AG. It was desired to know the position of the mail cart to assist in locating lost, or misplaced cart by the mail center staff. A simulated model was construed and the UKF applied to the TOA k-nearest neighbors trilateration data. In the simulation it was assumed the carts move at a constant velocity and their position is interpolated using Newtonian motion. It was found the application of the UKF greatly improved system performance.

The most direct comparison to this work is presented in [10], which describes the application of Kalman filters to a commercial RFID RTLS, in this case the ultra-wide band based Ubisense localization system. This system advertises centemeter level accuracy and uses a combination of TOA/TDOA/AOA methods. Real-world data was collected and filtered using two setups with a moving tag on a train track. It was found the KF improved system performance by up to 15%.

The UKF may also be applied to other localization technologies. In [11] a real world ultrasonic sensor system similar to the MITE Cricket. A UKF and pre-filtering stage were developed and applied to the real world system. It was found the filter performs better then the previously used EKF and provides a lower root-mean square error. [12] applies sigma-point filters to wi-fi based patient tracking within a elder care facility. A base filter, as well as pre-and post-filtering smoothers were developed and a random walk model for human movement was applied. The sigma-point kalman filter was shown to outperform the existing EKF methods.

Robotics also makes use of the Kalman filter as in [13], where the UKF and EKF are applied to a simulated model of robot movement using both laser range-finder and RFID based localization methods. It was found that the range-finder behavior was highly non-linear and would benefit from a more complex filtering implementation, however; the RFID

localization was well served by the Kalman filters with the UKF outperforming the EKF. Generalized sigma-point Kalman filters may also be applied to other GPS based localization models. In [14, 15] a GPS receiver and simple model radio controlled helicopter are evaluated. The performance of the UKF was compared against existing methods including the EKF and Iterative Least Squares measurements and found to display superior performance and stability.

4 Linear Kalman Filters

The KF, also known as a linear quadratic estimation, is a regressive filtering algorithm which attempts to find an optimal estimate of the underlying state of a system defined by a linear stochastic difference equation:

$$x_k = Ax_{k-1} + Bu_{k-1} + w_{k-1} \tag{1.5}$$

With system measurement, $z \in \mathbb{R}$, as:

$$z_k = Hx_k + v_k \tag{1.6}$$

Where x_k is the system state at time k, A is the state transition matrix, u are the state control variables, B is the control matrix, H is the measurement transition matrix, and v and w are the measurement and process noise respectively. w and v are assumed to be independent, white noise, with normal probability distributions:

$$p(w) \sim N(0, Q) \tag{1.7}$$

$$p(v) \sim N(0, R) \tag{1.8}$$

Where Q and R are the process and measurement noise covariance matrices respectively. Q, R, A, and H, could be constant, or change with each measurement update. Here we assume they are constant.

KF processing can be divided into two main phases, the predict phase, and the update

phase. During the predict phase the algorithm predicts a new sample based on the previous sample and an estimation filter. During the update phase the filter refines this estimate based on a new sample being acquired from the system. The estimated filter parameters are then updated and the filter loops back to predict the next sample. The equations for each phase are as follows:

Prediction Phase:

$$\hat{x}_k^- = A\hat{x}_{k-1} + Bu_{k-1} \tag{1.9}$$

$$P_k^- = AP_{k-1}A^T + Q \tag{1.10}$$

Update Phase:

$$K_k = P_k^- H^T (HP_k^- H^T + R)^{-1} \tag{1.11}$$

$$\hat{x}_k = \hat{x}_k^- + K_k(z_k - H\hat{x}_k^-) \tag{1.12}$$

$$P_k = (I - K_k H)P_k^- \tag{1.13}$$

Where: $\hat{x}$ is the estimated state, P is the state variance matrix (i.e., error of estimation), and K is the Kalman gain,

5 Non-Linear Kalman Filter

The classic KF described above is applicable only to linear systems. In cases where the system is non-linear, either in the measurement function, prediction (transition) function, or both, a separate class of KF must be used. The Unscented Kalman filter (UKF) and Extended Kalman filter (EKF) are the most common non-linear variants.

5.1 Extended Kalman Filter

The EKF is the first and most direct application of the Kalman filter to non-linear systems. This filter model attempts to allow for system non-linearities by linearizing the system through the use of Jacobian matrices[8]. This takes the form of a minimum mean-square-error estimator based on the first-order Taylor series expansion [16][11]. The EKF filter

equations are as follows:

Prediction Phase:

$$\hat{x}_k^- = f(\hat{x}_{k-1}, u_{k-1}, 0) \tag{1.14}$$

$$P_k^- = A_k P_{k-1} A_k^T + W_k Q_{k-1} W_k^T \tag{1.15}$$

Update Phase:

$$K_k = P_k^- H_k^T (H_k P_k^- H_k^T + V_k R_k V_k^T)^{-1} \tag{1.16}$$

$$\hat{x}_k = \hat{x}_k^- + K_k(z_k - h(\hat{x}_k^-, 0) \tag{1.17}$$

$$P_k = (I - K_k H_k) P_k^- \tag{1.18}$$

Where h, f : The non-linear measurement functions, $\hat{x}$: Estimated state, $\hat{x}_k^-$: Current state prediction, u : Control variables, P : State variance matrix (i.e., error of estimation), Q : Process variance matrix (i.e., error due to process), z : Measurement variables, K : Kalman gain, R : Measurement variance matrix (i.e., error from measurements). A : The Jacobian matrix of partial derivatives of f with respect to x, W : The Jacobian matrix of partial derivatives of f with respect to w, H : The Jacobian matrix of partial derivatives of h with respect to x, V : The Jacobian matrix of partial derivatives of h with respect to v. Subscripts are as follows: k current time period, $k-1$ previous time period.

The EKF is an effective adaptation of the Kalman filter to non-linear systems, however; it is known to induce large errors in certain non-linear systems. This is because the EKF only utilizes the first order terms of the Taylor series expansion as shown in Eq (1.19). The defect is most evident when the EKF is used on highly non-linear systems[11]. In these instances the first order Taylor series expansion is insufficient to adequately capture the behavior of the system to within a tolerable allowance. The system begins to diverge, leading to filter and system instability. For this reason the EKF has largely been replaced by the Sigma-Point family of Kalman filters as they do not exhibit this short coming.

$$f(x_k) = f(\hat{x}_k^-) + \left.\frac{\partial f(x_k)}{\partial x_k}\right|_{x=\hat{x}_k^-} \times (x_k - \hat{x}_k^-) \tag{1.19}$$

$$h(x_k) = h(\hat{x}_k^-) + \left.\frac{\partial h(x_k)}{\partial x_k}\right|_{x=\hat{x}_k^-} \times (x_k - \hat{x}_k^-) \tag{1.20}$$

5.2 Sigma-Point Kalman Filters

The family of sigma-point Kalman filters differ from that of the EKF in that they attempt to mitigate a non-linear system by manipulating system statistical variables, instead of the attempting to linearize the system itself. There are two main types of sigma-point based Kalman filters: the Unscented Kalman filter, and the Central Difference Kalman filter [17]. Unscented Kalman filters are discussed and used in this paper.

5.2.1 Unscented Kalman Filter

The UKF attempts to solve the issue of non-linearities by relying on a set of statistical random variables, sigma-points, and mapping those variables through the non-linearity using the unscented transformation (UT) [18]. The basis of the idea is that is it easier to approximate the non-linear transformation of a Gaussian distribution, than it is to approximate the transformation itself. The UKF has been shown by numerous authors to be superior to the EKF in performance [11, 8, 13, 19, 14, 20], reducing the positional error percentage by as much as 64% in some cases over the EKF [8].

The UT is a method of calculating the statistics of a random variable which undergoes a non-linear transformation[18]. The basis of the idea is that is it easier to approximate the non-linear transformation of a Gaussian distribution, then it is to approximate the transformation itself. The UT works by taking a set of known statistical points (commonly the mean and covariance) and passes each through the non-linear transformation. The transformed points can then be used to approximate the state of the transformed random variable without actually approximating the non-linearity itself.

The points used by the UT are known as *sigma points*. The selection algorithm for determining the sigma points is chosen to provide at least second order information of the

underlying non-linearity. This results in points located at the mean, and symmetrically along the axis of covariance, with two points in each dimension[9]. For the n-dimensional random variable x, with mean $\bar{x}$ and covariance $\mathbf{P}_{xx}$, $2n+1$ sigma points and associated weights are given by the following:

$$\mathcal{X} = \bar{x} \qquad W_0 = \kappa/(n+\kappa) \tag{1.21}$$

$$\mathcal{X}_i = \bar{x} + \left(\sqrt{(n+\kappa)\mathbf{P}_{xx}}\right)_i \qquad W_i = 1/2(n+\kappa) \tag{1.22}$$

$$\mathcal{X}_{i+n} = \bar{x} - \left(\sqrt{(n+\kappa)\mathbf{P}_{xx}}\right)_i \qquad W_{i+n} = 1/2(n+\kappa) \tag{1.23}$$

Where $\kappa \in \Re$, $\left(\sqrt{(n+\kappa)\mathbf{P}_{xx}}\right)_i$ is the ith row or column of the matrix square root of $(n+\kappa)\mathbf{P}_{xx}$, and W_i is the weight associated with the ith point. Once the sigma points for a given system are determined they are propagated through the non-linearity as:

$$\mathcal{Y}_i = f[\mathcal{X}_\mathbf{i}] \tag{1.24}$$

The new transformed mean and covariance are then calculated using the weighted averages and outer product of the transformed sigma points:

$$\bar{y} = \sum_{i=0}^{2n} W_i \mathcal{Y}_i \tag{1.25}$$

$$\mathbf{P}_{yy} = \sum_{i=0}^{2n} W_i \left\{\mathcal{Y}_i - \bar{y}\right\} \left\{\mathcal{Y}_i - \bar{y}\right\}^T \tag{1.26}$$

The UKF takes the methodology of the unscented transformation, and applies it to the basic KF structure [9]. Assuming an n-dimensional input of a Gaussian position estimate:

$$\bar{x}_{t-1} = E[x_{t-1}] \tag{1.27}$$

$$\mathbf{P}_{t-1} = E[(x_{t-1} - \bar{x}_{t-1})(x_{t-1} - \bar{x}_{t-1})^T] \tag{1.28}$$

First the sigma-points of the previous time step are calculated as:

$$\mathcal{X}_{t-1} = \begin{bmatrix} \bar{x}_{t-1} & \bar{x}_{t-1} + \gamma\sqrt{\mathbf{P}_{t-1}} & \bar{x}_{t-1} - \gamma\sqrt{\mathbf{P}_{t-1}} \end{bmatrix} \tag{1.29}$$

Where $\gamma = \sqrt{n+\delta}$ and $\delta = \alpha^2(n+\kappa) - n$ with α and κ as scaling parameters, and n as the dimension of the state space. The calculated sigma points are then passed through the non-linear control function, f, to find the transformed sigma-points, mean, and covariance as:

$$\mathcal{X}_t^* = f(\bar{x}_t, \mathcal{X}_{\mathbf{t-1}}) \tag{1.30}$$

$$\bar{x}_t^* = \sum_{i=0}^{2n} w_m^i \mathcal{X}_t^{*[i]} \tag{1.31}$$

$$\bar{\mathbf{P}}_t = \sum_{i=0}^{2n} w_c^i \left(\mathcal{X}_t^{*[i]} - \bar{x}_t^*\right)\left(\mathcal{X}_t^{*[i]} - \bar{x}_t^*\right)^T + \mathbf{R} \tag{1.32}$$

Where $\mathbf{R}$ is the covariance of the process noise, t is the current time sample, $\mathcal{X}^*$ are the transformed sigma points, and w_m and w_c are weights calculated as:

$$w_m^0 = \frac{\delta}{n+\delta} \tag{1.33}$$

$$w_c^0 = \frac{\delta}{n+\delta} + \left(1 - \alpha^2 + \beta\right) \tag{1.34}$$

$$w_m^i = w_c^i = \frac{1}{2\left(n+\delta\right)} \qquad \text{for } i = 1, \ldots, 2n \tag{1.35}$$

With β as a scaling parameter. Using the newly calculated $\bar{x}_t^*$ and $\bar{\mathbf{P}}_t$, a new set of sigma-points are calculated as:

$$\mathcal{X}_t = \begin{bmatrix} \bar{x}_t^* & \bar{x}_t^* + \gamma\sqrt{\bar{\mathbf{P}}_t} & \bar{x}_t^* - \gamma\sqrt{\bar{\mathbf{P}}_t} \end{bmatrix} \tag{1.36}$$

The sigma-points are then used to determine a predicted observation, $\hat{z}_t$, with uncertainty, $\mathbf{S}_t$, through the non-linear measurement function, h, as:

$$\mathbf{Z}_t = h(\mathcal{X}_t) \tag{1.37}$$

$$\hat{z}_t = \sum_{i=0}^{2n} w_m^i \mathbf{Z}_t^i \tag{1.38}$$

$$\mathbf{S}_t = \sum_{i=0}^{2n} w_c^i \left(\mathbf{Z}_t^i - \hat{z}_t\right)\left(\mathbf{Z}_t^i - \hat{z}_t\right)^T + \mathbf{Q} \tag{1.39}$$

Where $\mathbf{Q}$ is the covariance of the measurement noise. The Kalman gain, $\mathbf{K}_t$, and the cross-covariance, $\bar{\mathbf{P}}_t^{x,z}$, are then calculated as:

$$\bar{\mathbf{P}}_t^{x,z} = \sum_{i=0}^{2n} w_c^i \left(\mathcal{X}_t^i - \bar{x}_t^*\right) \left(\mathbf{Z}_t^i - \hat{z}_t\right)^T \tag{1.40}$$

$$\mathbf{K}_t = \bar{\mathbf{P}}_t^{x,z} \mathbf{S}_t^{-1} \tag{1.41}$$

Finally the outputs of the UKF, x_t and $\mathbf{P}_t$ are computed as:

$$\bar{x}_t = \bar{x}_t^* + \mathbf{K}_t(z_t - \hat{z}_t) \tag{1.42}$$

$$\mathbf{P}_t = \bar{\mathbf{P}}_t - \mathbf{K}_t \mathbf{S}_t \mathbf{K}_t^T \tag{1.43}$$

Chapter 2

Modeling Approach

The CSL RTLS used provides two sets of data output suitable for our model. The first are the raw distance measurements obtained using TOA. The TOA calculation is computed automatically by the system, and the TOA distance from the receiver to the tag, d_m, is calculated and made available through the PC interface. This measurement is transformed into a (x, y) localization using a non-linear transformation. Because of this non-linearity, the mathematical model of the measurement function, h, is non-linear, and a non-linear form of the KF must be used.

The second set of data available to us is the final (x, y) localization computed by the RTLS system. In this case the system has chosen the two receivers with the highest RSSI measurement, computed their TOA distance, and then performed the non-linear computations to obtain a final localization. As the system has already processed the non-linearity, the mathematical model of the measurement function, h, is linear and the normal KF may be used.

1 Linear Kalman Filter Design

The first step in designing the KF was to create a system function, f, based on the known system characteristics as needed by (1.9). The control variables of interest are the (x, y) position of a tag in a given 2D Cartesian space. Based on this we assume a third-order position, velocity, acceleration, model of motion of a given tag, where P_t, V_t, and a_t are the position, velocity, and acceleration of a given tag respectively, and Δt is the sample time.

$$P_t = P_{t-1} + V_{t-1}\Delta t + \frac{1}{2}a_{t-1}(\Delta t)^2 \tag{2.1}$$

This equation is captured in the state control vector, Θ:

$$\Theta_t = \begin{bmatrix} x_t & y_t & V_t^x & V_t^y & a_t^x & a_t^y \end{bmatrix}^T \tag{2.2}$$

Our general system function, f, may then be written in a matrix form as:

$$f(\Theta_t, \Theta_{t-1}) = A\Theta_{t-1} + w_{t-1} \tag{2.3}$$

Where A is the state transition matrix defined as:

$$A = \begin{bmatrix} 1 & 0 & \Delta t & 0 & \frac{1}{2}(\Delta t)^2 & 0 \\ 0 & 1 & 0 & \Delta t & 0 & \frac{1}{2}(\Delta t)^2 \\ 0 & 0 & 1 & 0 & \Delta t & 0 \\ 0 & 0 & 0 & 1 & 0 & \Delta t \\ 0 & 0 & 0 & 0 & 1 & 0 \\ 0 & 0 & 0 & 0 & 0 & 1 \end{bmatrix} \tag{2.4}$$

w is the process noise and Q_n is the additive process noise for each measurement respectively as:

$$w_{t-1} = \begin{bmatrix} Q_x & Q_y & Q_{x_V} & Q_{y_V} & Q_{x_a} & Q_{y_a} \end{bmatrix}^T \tag{2.5}$$

As the only measured value is that of position, we may assume there is no process noise associated with V or a and thus w reduces to:

$$w_{t-1} = \begin{bmatrix} Q_x & Q_y & 0 & 0 & 0 & 0 \end{bmatrix}^T \tag{2.6}$$

As there is no translation between a measured sample and the input to the state transition matrix, the measurement matrix, H, is simply an identity mapping of the (x, y) input:

$$H = \begin{bmatrix} 1 & 0 & 0 & 0 & 0 & 0 \\ 0 & 1 & 0 & 0 & 0 & 0 \end{bmatrix} \tag{2.7}$$

2 Non-linear Kalman Filter (UKF) Design

The UKF was chosen for use as opposed to the EKF because of its relative ease of computation (no Jacobian calculations), and because of its superior performance compared to the EFK [11, 8, 13, 19, 14, 20]. The system function, f, state transition matrix, A, and process noise, w, are identical to the KF. The difference occurs in the non-linear measurement function, h. In this case h must transform the TOA distance distance measurements into (x, y) coordinates:

$$h_t = \begin{bmatrix} \sqrt{(X_r^1 - x_t)^2 + (Y_r^1 - y_t)^2} \\ \sqrt{(X_r^2 - x_t)^2 + (Y_r^2 - y_t)^2} \end{bmatrix} + v_t \tag{2.8}$$

Where x_t and y_t are the (x, y) coordinates of the tag, X_r^n and Y_r^n are the static (x, y) coordinates of the readers, and v_t is the measurement noise as:

$$v_t = \begin{bmatrix} R_{d_1} & R_{d_2} \end{bmatrix}^T \tag{2.9}$$

Where R_{d_n} is the additive measurement noise associated with each receiver-tag pair distance reading. Based on h, our measurement vector, $\mathbf{Z}$, may then be written as:

$$\mathbf{Z}_t = \begin{bmatrix} d_1 \\ d_2 \end{bmatrix} = \begin{bmatrix} \sqrt{(X_r^1 - x_t)^2 + (Y_r^1 - y_t)^2} \\ \sqrt{(X_r^2 - x_t)^2 + (Y_r^2 - y_t)^2} \end{bmatrix} + \begin{bmatrix} R_{d_1} \\ R_{d_2} \end{bmatrix} \tag{2.10}$$

Where d_n is the TOA distance distance reading for each of the reader-tag pairs.

Chapter 3

Experimental Setup

1 RTLS Experimental Setup

The CSL RTLS was set up in two indoor testing locations in order to collect data for analysis. Two locations were chosen to provide different testing conditions and environmental characteristics.

1.1 Experimental Setup - Test Site 1

Test site 1 was an indoor laboratory with cinder-block walls, a corrugated metal ceiling (approximately 20 ft height), and windows on two ends of the lab. To simulate an office environment, and also provide low-level RFID interference, four metal desks each with a PC, a small conference table made of wood with a metal base, office chairs, and a large metal filing cabinet were placed in the lab. Four anchors, one master and three slaves, were used and placed in a rectangle around the perimeter of the space with one anchor at each corner as shown in Figure 3.1.

Each anchor was mounted on a metal tripod at an elevation of 2 m in order to ensure a clear line-of-sight across the entire tracking area. The anchors were aimed into the middle of the rectangular tracking area at an azimuth of 45 degrees and an attitude of -20 degrees from horizontal. The anchors used were CSL part number CS5114 (master anchor) and CS5112 (slave anchors) wide beam receivers with an 180-degree antenna angle. The tag used was a CSL part number CS3151TC battery-powered active asset tag with on-board temperature, motion, and battery monitoring.

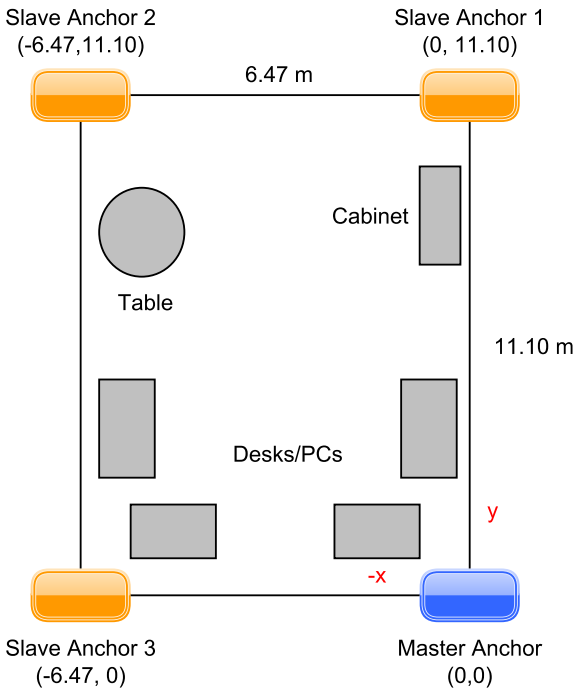

Figure 3.1: Test Site 1- CSL RTLS experimental setup

1.2 Experimental Setup - Test Site 2

Test site 2 was an indoor industrial space with cinder-block and drywall walls, a wooden beam ceiling 3.91 m high, windows along one wall, and two large wooden support beams in the middle of the space. The space was used as a general lab and had multiple tables, chairs, and workspaces throughout. Four anchors, one master and three slaves, were used and placed in a rectangle around the perimeter of the space with one anchor at each corner as shown in Figure 3.2.

Each anchor was mounted on a metal tripod at an elevation of 1.95 m in order to ensure a clear line-of-sight across the entire tracking area. The anchors were aimed into the middle of the rectangular tracking area at an azimuth of 45 degrees and an attitude of -20 degrees from horizontal. The anchors and tag were the same as used in test environment 1.

The RF environment of test site 2 was also characterized using a portable RF spectrum analyzer. This was done to observe if there was excessive noise or other signals present in the RTLS system operating frequency band which could impact the testing and noise

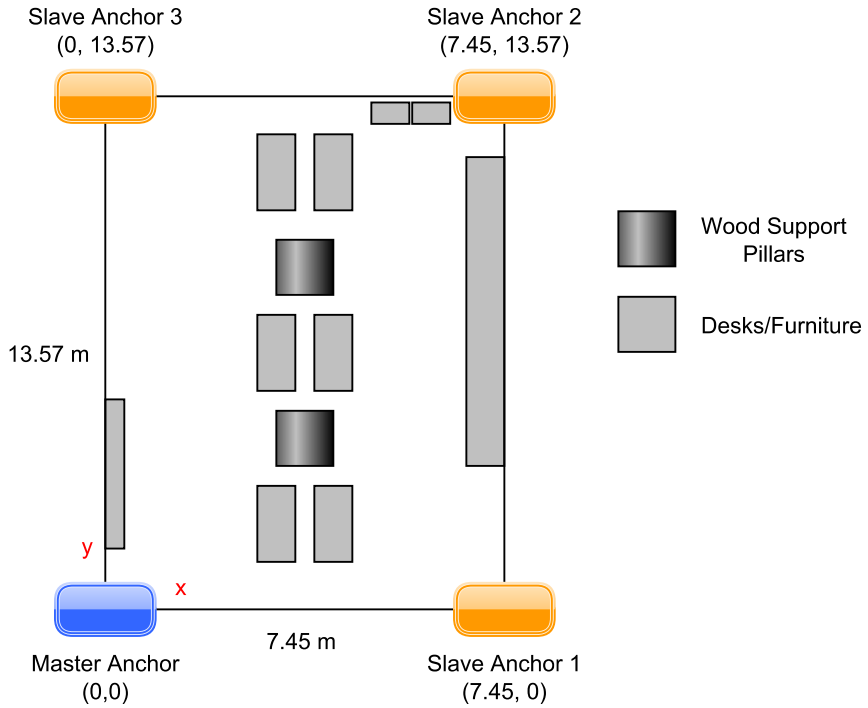

Figure 3.2: Test Site 2 - CSL RTLS experimental setup

behavior of the system. The RTLS system operates in the 2.4 GHz ISM band, which is also used by most Wireless LAN (WiFi) networks. The test site was covered by multiple wireless networks so noise in this band was to be expected.

The spectrum analyzer was set up in the testing environment and spectrograms taken of the 2.4 GHz ISM band from 2.3 GHz to 2.5 GHz. Spectrograms were taken with the RTLS system off, and then on shown in Figure 3.3 and 3.4.

1.3 Data Collection and Filtering

Data was collected using the CSL RTLS PC software package and a custom MySQL database. Data samples were captured and saved into an Excel spreadsheet. The Excel data was formated in sets of 4 readings, each reading corresponding to one anchor, and then entire set of 4 making up a single system sample. Each reading included the sample number, tag ID, UL RSSI (RSSI from tag to anchor), DL RSSI (RSSI from anchor to tag), and TOA distance measurement for each tag/reader pair, reported tag coordinates,

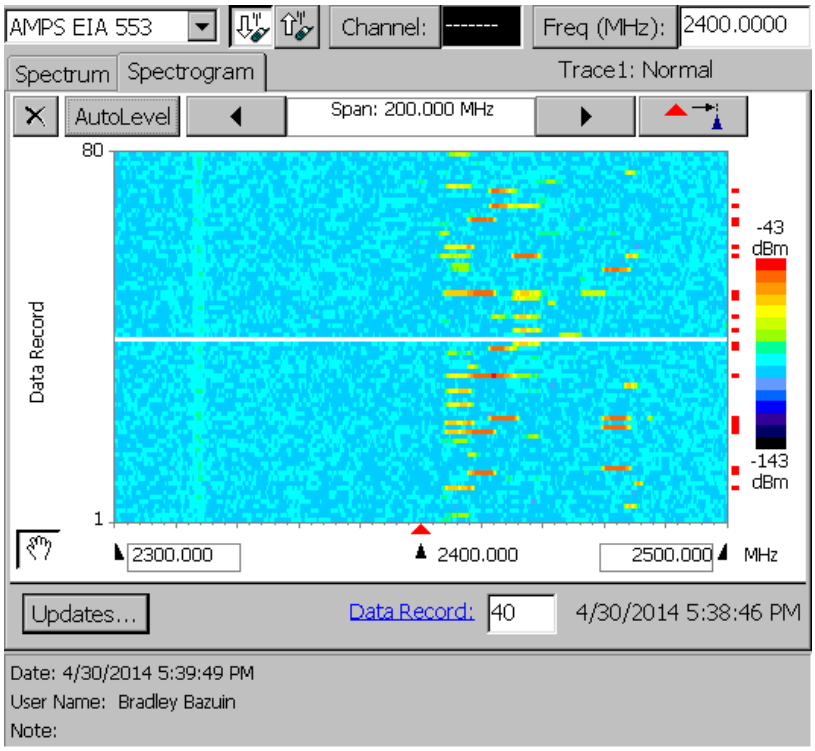

Figure 3.3: Spectrogram taken at test site 2 of the 2.4 GHz ISM band with the RTLS system off showing ambient RF activity in the band

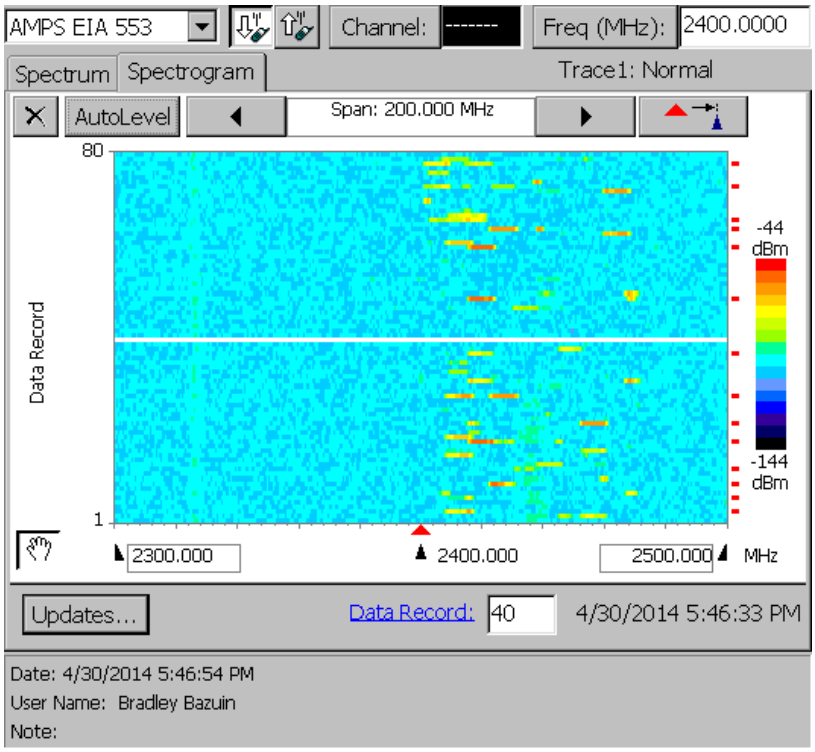

Figure 3.4: Spectrogram taken at test site 2 of the 2.4 GHz ISM band with the RTLS system on showing RF activity in the band both from ambient sources and the RTLS system

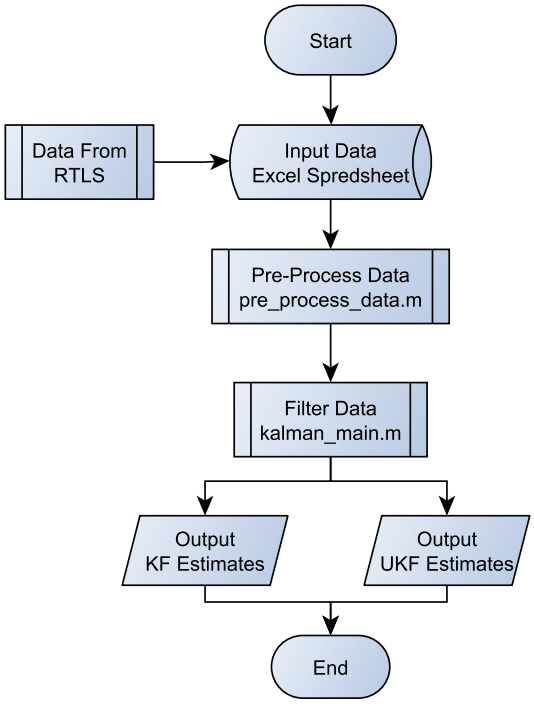

Figure 3.5: Overall system processing flowchart

and sample timestamp. The sample rate, Δt, of the RTLS system for all tests was 1 s. The collected data samples were pre-processed using Matlab before applying the filtering techniques. Figure 3.5 shows the overall system flowchart.

The pre-processing step converted the raw Excel data into an easy to manage format in Matlab and computed the usable sample size and measurement noise variance. Figure 3.6 shows the pre-processing flowchart.

First the sample data to be used by the filtering processes was extracted from the raw Excel data. For the KF the computed tag coordinates were used directly as reported by the software for each sample. For the UKF two TOA distance measurements were needed to compute the localization calculations. We followed the same method of anchor selection the RTLS system uses to determine which two anchor's distance measurements to use in the calculation. From the four TOA distance measurements captured per sample, the two associated with the highest RSSI value were selected for use. The RTLS system reports RSSI values from 0-25, with 0 representing the highest RSSI, and 25 representing the lowest RSSI. Dynamically selecting the anchors used in each recursion for the UKF allowed us to

use the best data for each sample, helping to mitigate possible line-of-site or interference errors affecting other anchors.

The RTLS system output sometimes reported a bad or unavailable reading due to interference or a failed RFID read attempt. This was indicated in the Excel output by a RSSI value of 127. When pre-processing the data we watched for these error readings and excluded them from the calculations. Any one or multiple of the 4 anchor readings could report a bad reading. If 2 or fewer readers reported an error the sample could still be used, however; if more then 2 readers reported an error the entire sample had to be discarded as there was insufficient data to compute the TOA localization.

The last step in pre-processing was then to compute the sample measurement noise variance, R, used by the filtering algorithms. This was calculated as the normalized data set variance in each axis as in:

$$\sigma^2 = \frac{1}{n-1} \sum_{i=1}^{n} (x_i - \bar{x}_i)^2 \tag{3.1}$$

Where x_i is the localization output and $\bar{x}_i$ is the mean of the localization output for sample i of n total samples. For the KF the x and y coordinate sample data variance was used. For the UKF the variance of the sample data TOA distance measurements for each reader was used.

The pre-processed data was then filtered through the KF and UKF algorithms using Matlab and the EKF/UKF Toolbox for Matlab [21]. Figure 3.7 shows the Kalman filtering Matlab code flowchart. For the KF algorithm the measurement noise variance calculated during pre-processing was applied to all KF recursions. In the case of the UKF, however; from the four measurement noise variances calculated during pre-processing, the two variances associated with the anchors selected for the current recursion of the UKF algorithm were used. Dynamically selecting the measurement noise variance per recursion for the UKF allowed us to tailor each recursion to the particular anchors used, eliminating the effects of other, possibly non-line-of-sight, and thus higher variance, anchors.

Despite the sample rate of the system being 1 s, a sample rate of 100 ms was used in the Matlab simulations. This was found empirically to constrain the high variance in the

RTLS system output by dampening the response of the state transition matrix, A. This lead to a more accurate filter output with lower variance.

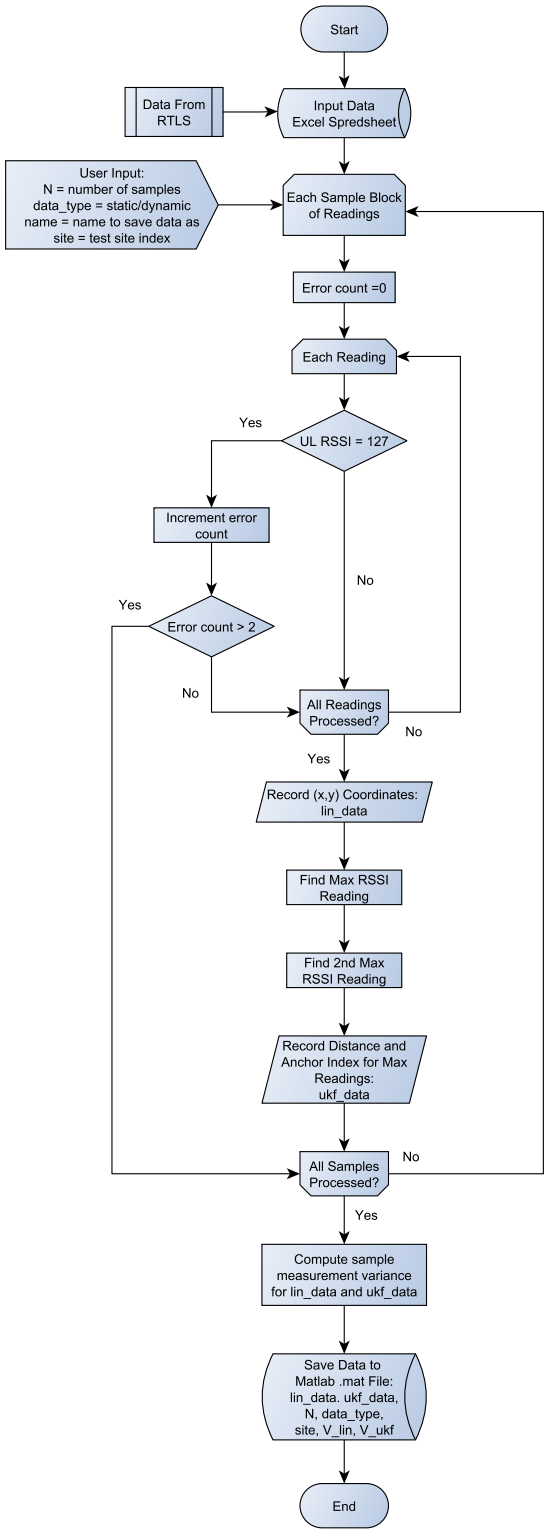

Figure 3.6: Matlab data pre-processing flowchart

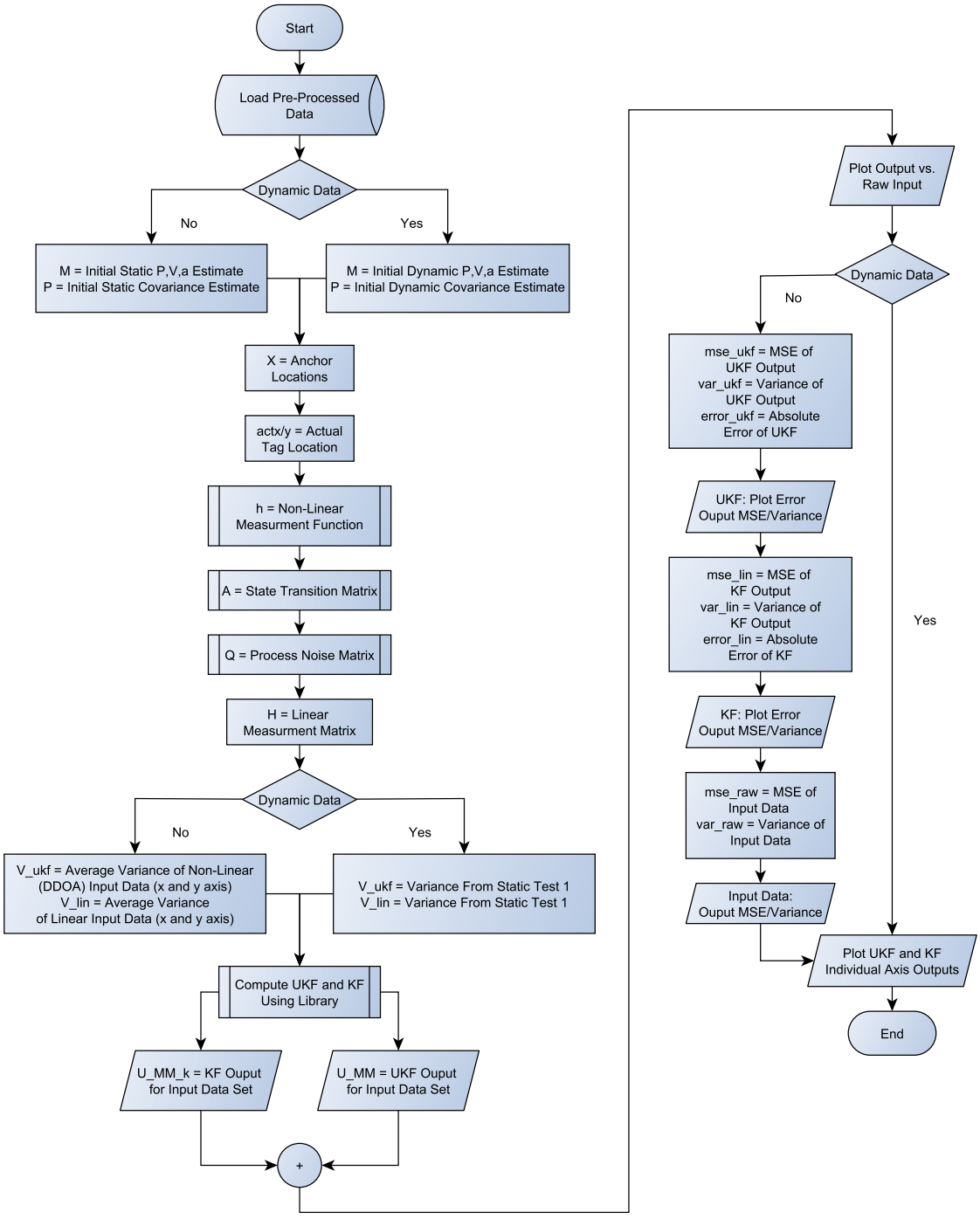

Figure 3.7: Matlab kalman filter processing flowchart

Chapter 4

Results

1 Static Testing - Test Site 1

Two data sets were collected, each with a single tag located at a static coordinate within the tracking area. Table 4.1 shows the tag positions for each test. 100 data samples were taken for Test 1, and 50 for Test 2. Tracking results are shown in Figure 4.1, 4.2 and 4.3.

The measurement noise variance, R, was calculated by the pre-processing step and used directly. The calculated R values are shown in Table 4.2 and 4.3. The process noise, Q, was empirically set to $1{\times}10^{-15}$ as there is no inherent noise in the system process. There could be noise induced by the CSL RTLS system or software itself but this is unknown and was ignored.

The initial localization estimate was chosen to be roughly the center of the tracking area at $(-3.2, 5.5)$ with zero velocity and acceleration to give all tests a common, non-biased starting estimate. Initial covariances were empirically chosen selecting 10 for the localization estimate, indicating low confidence in this estimate, and $1{\times}10^{-15}$ for the velocity and acceleration estimates, indicating high confidence in these estimates (we know the tag is stationary). The velocity and acceleration covariance is chosen very small instead of zero because the covariance matrix must be positive definite. The resulting initial state and

Table 4.1: Test Site 1 - Static tag locations

Test	x (m)	y (m)	z (m)
1	-3.35	4.67	1.20
2	-2.75	8.08	0.49

Table 4.2: Test Site 1 - KF measurement noise for static sample data sets

Test	Axis	R
1	x	.0889
	y	.6242
2	x	.0716
	y	.0633

Table 4.3: Test Site 1 - UKF anchor TOA distance measurement noise for static sample data sets

	R			
Test	Master	Slave 1	Slave 2	Slave 3
1	.3855	.0422	.0547	.0651
2	.1399	.0455	.0480	.0372

covariance estimates, $\bar{\theta}_{t-1}$ and $\mathbf{P}_{t-1}$, were then:

$$\bar{\theta}_{t-1} = \begin{bmatrix} -3.2 & 5.5 & 0 & 0 & 0 & 0 \end{bmatrix}$$

$$\mathbf{P}_{t-1} = \begin{bmatrix} 10 & 10 & 1 \times 10^{-15} & 1 \times 10^{-15} & 1 \times 10^{-15} & 1 \times 10^{-15} \end{bmatrix}$$

The mean square error (MSE) and variance for each test and each coordinate axis was calculated and shown in Table 4.4 and 4.5. The MSE, and variance were calculated as:

$$\text{MSE} = \frac{1}{n} \sum_{i=1}^{n} (\hat{x}_i - x_i)^2 \tag{4.1}$$

$$\sigma^2 = \frac{1}{n-1} \sum_{i=1}^{n} (x_i - \bar{x}_i)^2 \tag{4.2}$$

Where x_i is the localization output, $\hat{x}_i$ is the actual tag position, and $\bar{x}_i$ is the mean of the localization output for sample i of n total samples. To allow for the initial adaptation period seen in Figure 4.3 for each filter, the first 10 estimation outputs of the UKF and KF were ignored and not used in their respective MSE and variance calculations. All samples were used for the raw data MSE and variance calculations.

Table 4.4: Test Site 1 - MSE for static sample data sets

		MSE		
Test	Axis	Raw Data	KF	UKF
1	x	.1343	.0557	.1710
	y	.6307	.0693	1.4738
2	x	.1069	.0408	.2824
	y	.0675	.0042	.5965

Table 4.5: Test Site 1 - Variance for static sample data sets

		Variance - σ^2		
Test	Axis	Raw Data	KF	UKF
1	x	.0889	.0073	.0759
	y	.6242	.0200	.0259
2	x	.0716	.0010	.0007818
	y	.0633	.0017	.0008241

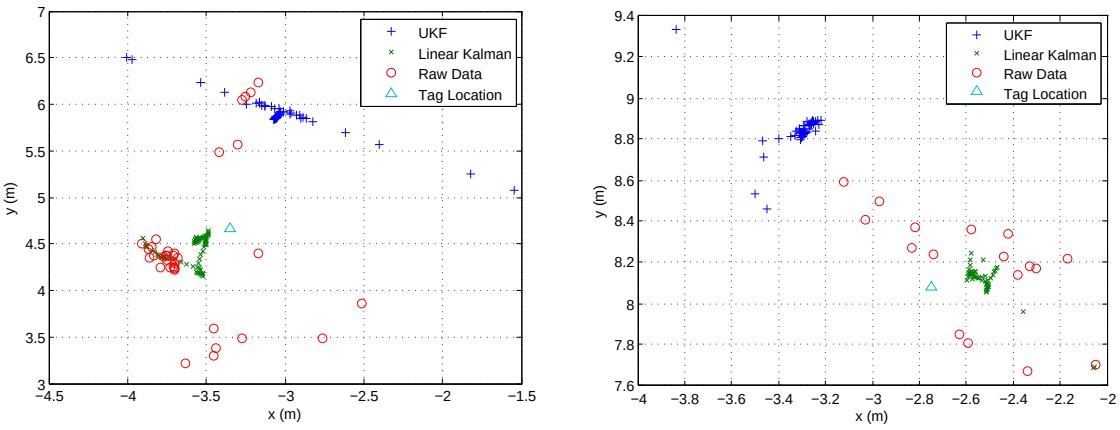

(a) Test 1

(b) Test 2

Figure 4.1: Static Tag Tests - Test Site 1: Filtering results using sample data from the CSL RTLS

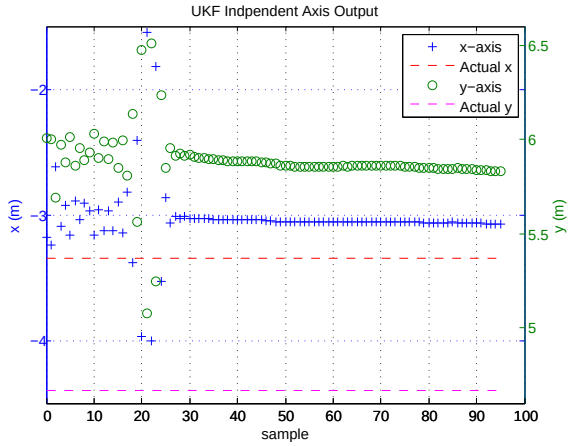

(a) Test 1 - Individual location axis output vs sample for UKF processing

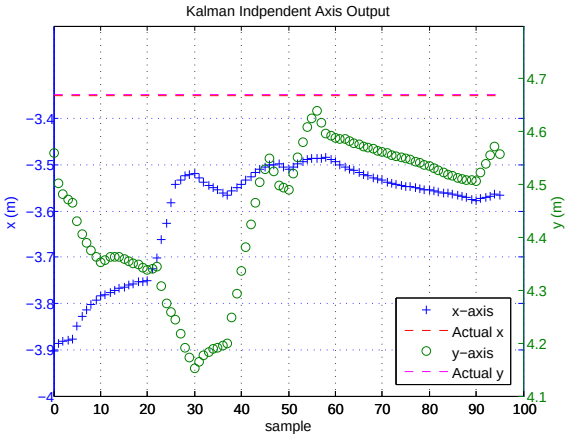

(b) Test 1 - Individual location axis output vs sample for KF processing

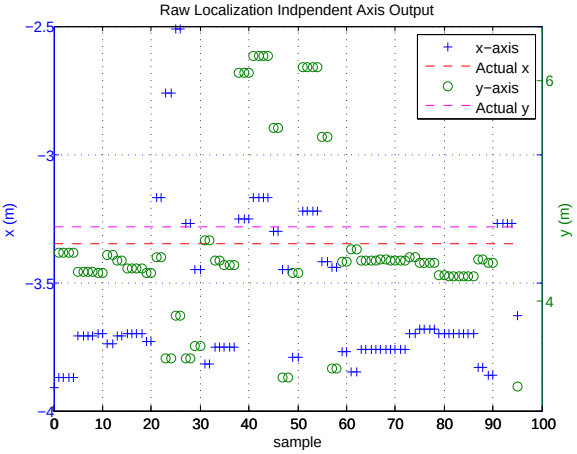

(c) Test 1 - Individual location axis output vs sample for raw localization data from the RTLS

Figure 4.2: Static Tag Test 1 - Test Site 1: Individual axis outputs of filters and RTLS system

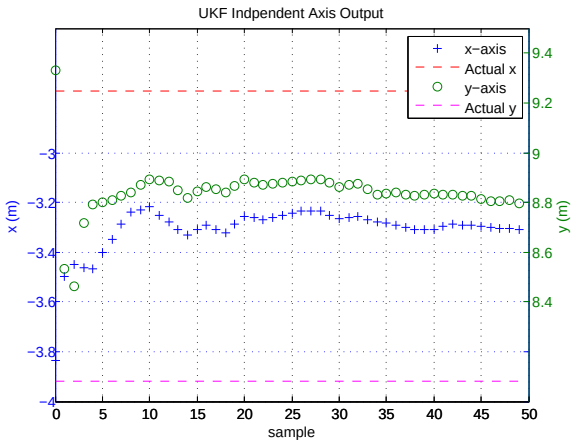

(a) Test 2 - Individual location axis output vs sample for UKF processing

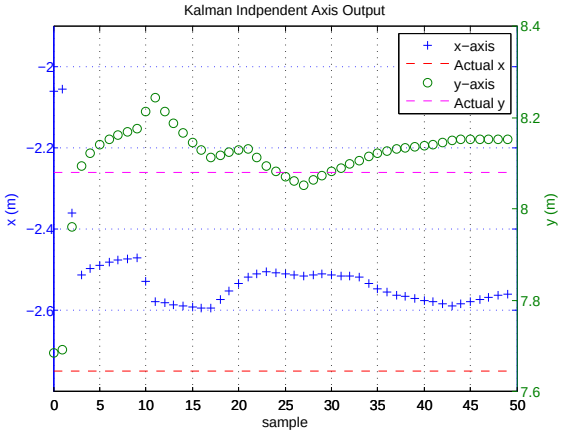

(b) Test 2 - Individual location axis output vs sample for KF processing

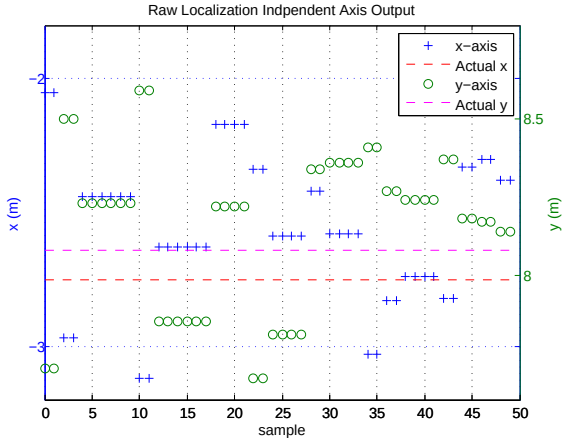

(c) Test 2 - Individual location axis output vs sample for raw localization data from the RTLS

Figure 4.3: Static Tag Test 2 - Test Site 1: Individual axis outputs of filters and RTLS system

2 Static Testing - Test Site 2

Six data sets were collected, each with a single tag located at a static coordinate within the tracking area. Table 4.6 and Figure 4.4 show the tag positions for each test. 250 data samples were taken for all tests. Tracking results are shown in Figure 4.5, 4.6- 4.11.

The measurement noise variance, R, was calculated by the pre-processing step and used directly. The calculated R values are shown in Table 4.7 and 4.8. The process noise, Q, was empirically set to 1×10^{-15} as there is no inherent noise in the system process. There could be noise induced by the CSL RTLS system or software itself but this is unknown and was ignored.

The initial localization estimate was chosen to be roughly the center of the tracking area at $(3.72, 6.78)$ with zero velocity and acceleration to give all tests a common, non-biased starting estimate. Initial covariances were empirically chosen selecting 10 for the localization estimate, indicating low confidence in this estimate, and 1×10^{-15} for the velocity and acceleration estimates, indicating high confidence in these estimates (we know the tag is stationary). The velocity and acceleration covariance is chosen very small instead of zero because the covariance matrix must be positive definite. The resulting initial state and covariance estimates, $\bar{\theta}_{t-1}$ and $\mathbf{P}_{t-1}$, were then:

$$\bar{\theta}_{t-1} = \begin{bmatrix} 3.72 & 6.78 & 0 & 0 & 0 & 0 \end{bmatrix}$$

Table 4.6: Test Site 2 - Static tag locations

Test	x (m)	y (m)	z (m)
1	3.31	6.68	1.20
2	5.24	6.74	1.20
3	6.33	9.72	1.20
4	6.21	3.43	1.20
5	1.44	3.83	1.20
6	1.36	9.06	1.20

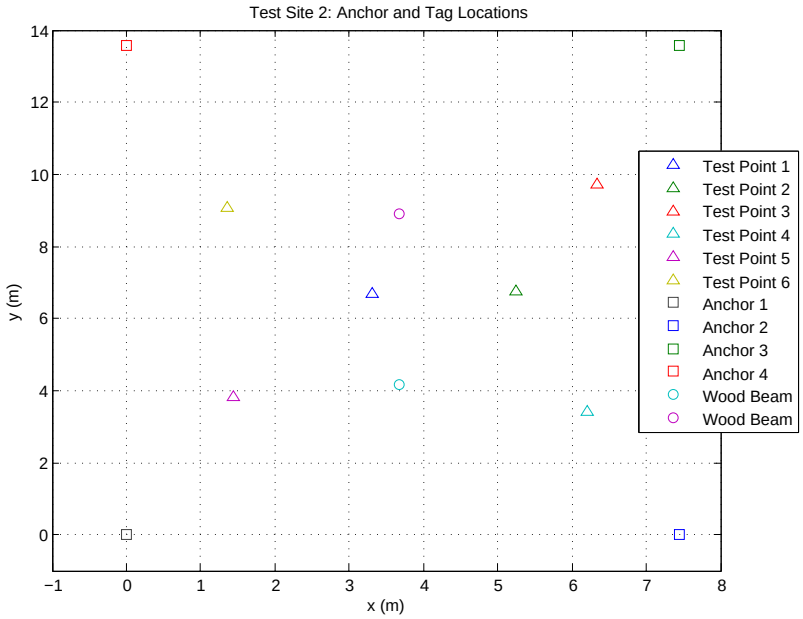

Figure 4.4: Test Site 2: Tag and anchor locations

Table 4.7: Test Site 2 - KF measurement noise for static sample data sets

Test	Axis	R
1	x	.0975
	y	.0326
2	x	.1669
	y	.0274
3	x	.0350
	y	.0253
4	x	.6419
	y	2.1448
5	x	.4452
	y	.1960
6	x	.1292
	y	.1517

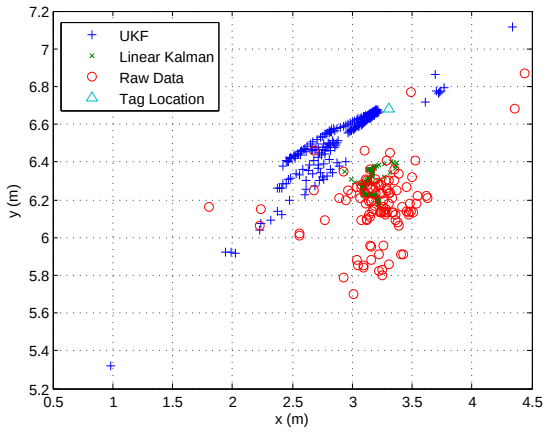

(a) Test 1

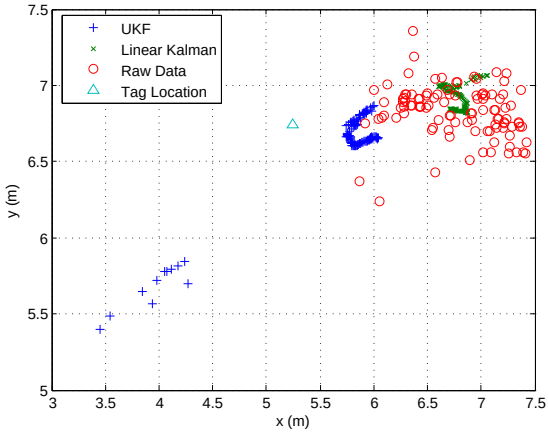

(b) Test 2

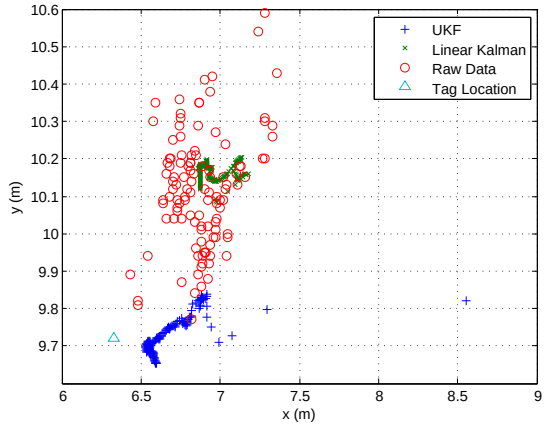

(c) Test 3

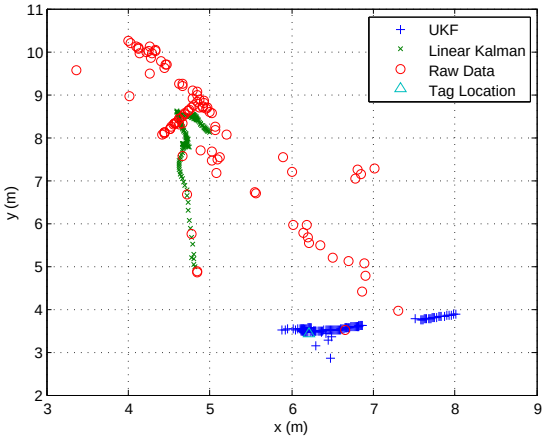

(d) Test 4

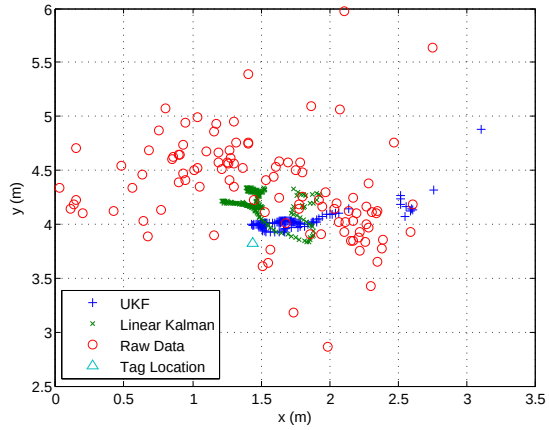

(e) Test 5

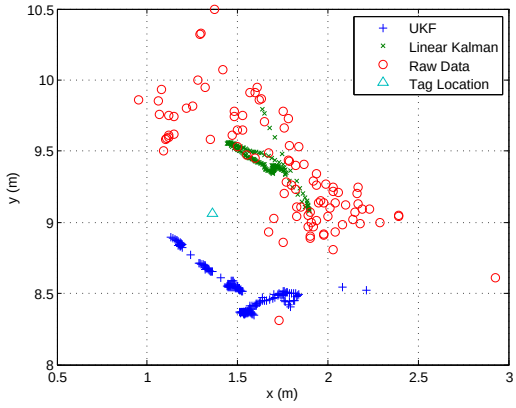

(f) Test 6

Figure 4.5: Static Tag Tests - Test Site 2: Filtering results using sample data from the CSL RTLS

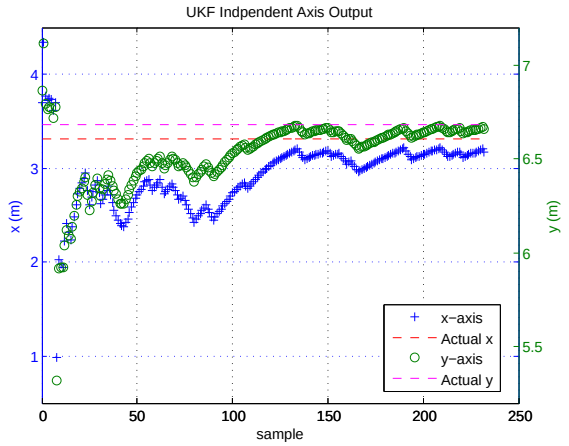

(a) Test 1 - Individual location axis output vs sample for UKF processing

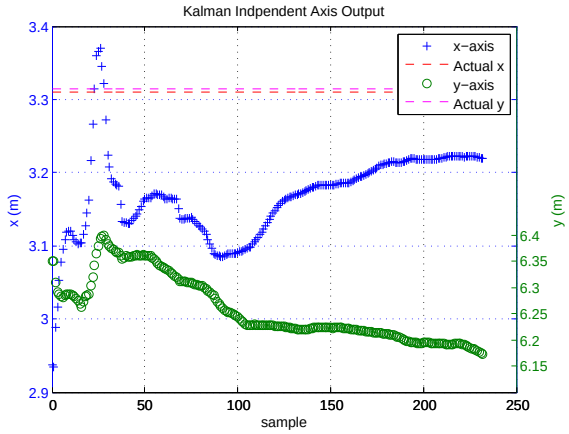

(b) Test 1 - Individual location axis output vs sample for KF processing

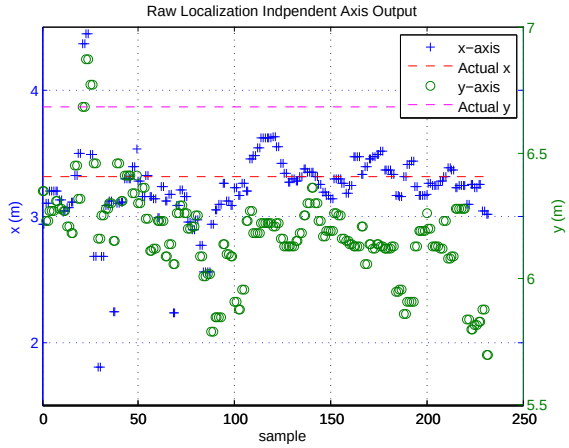

(c) Test 1 - Individual location axis output vs sample for raw localization data from the RTLS

Figure 4.6: Static Tag Test 1 - Test Site 2: Individual axis outputs of filters and RTLS system

(a) Test 2 - Individual location axis output vs sample for UKF processing

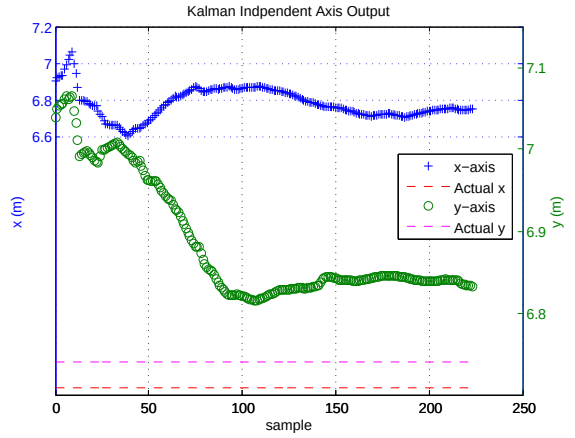

(b) Test 2 - Individual location axis output vs sample for KF processing

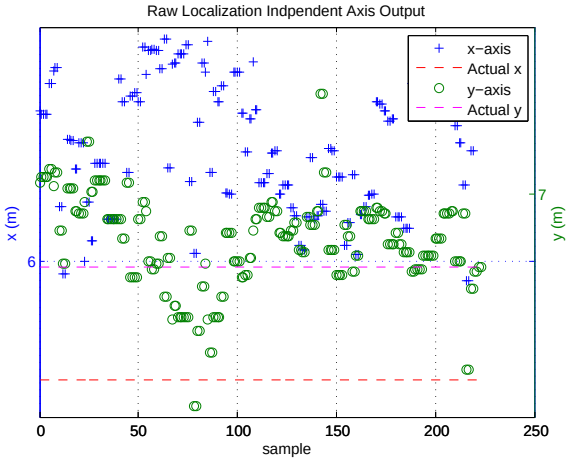

(c) Test 2 - Individual location axis output vs sample for raw localization data from the RTLS

Figure 4.7: Static Tag Test 2 - Test Site 2: Individual axis outputs of filters and RTLS system

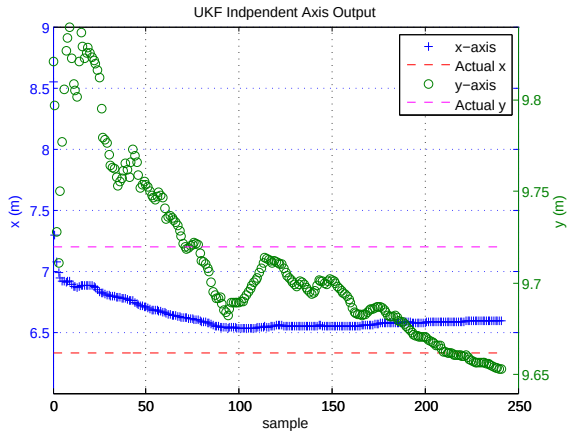

(a) Test 3 - Individual location axis output vs sample for UKF processing

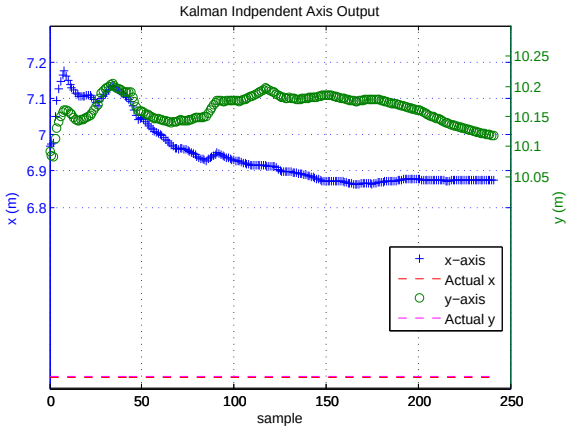

(b) Test 3 - Individual location axis output vs sample for KF processing

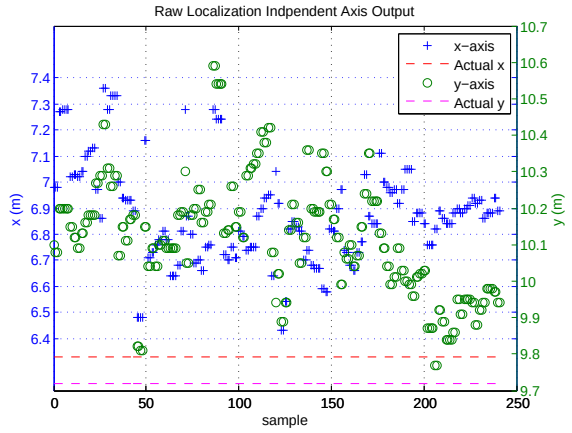

(c) Test 3 - Individual location axis output vs sample for raw localization data from the RTLS

Figure 4.8: Static Tag Test 3 - Test Site 2: Individual axis outputs of filters and RTLS system

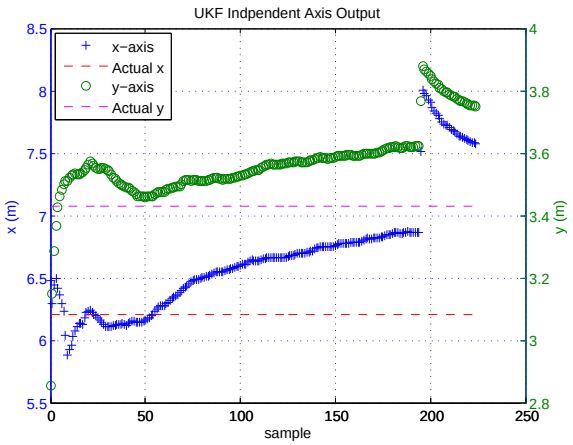

(a) Test 4 - Individual location axis output vs sample for UKF processing

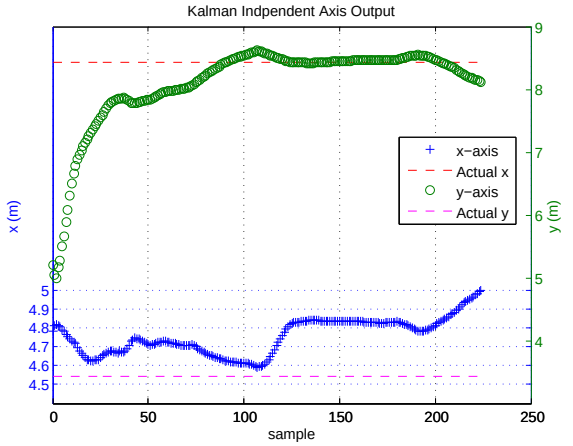

(b) Test 4 - Individual location axis output vs sample for KF processing

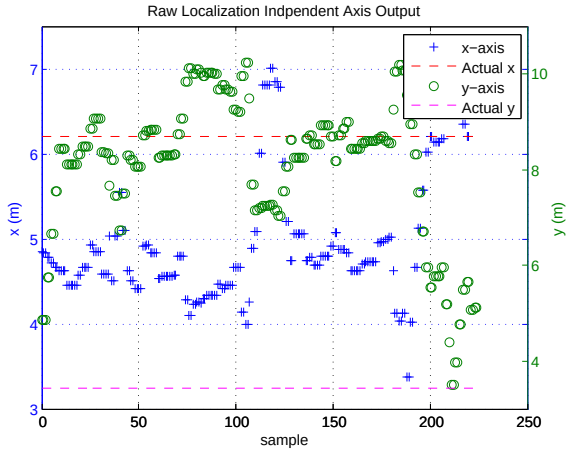

(c) Test 4 - Individual location axis output vs sample for raw localization data from the RTLS

Figure 4.9: Static Tag Test 4 - Test Site 2: Individual axis outputs of filters and RTLS system

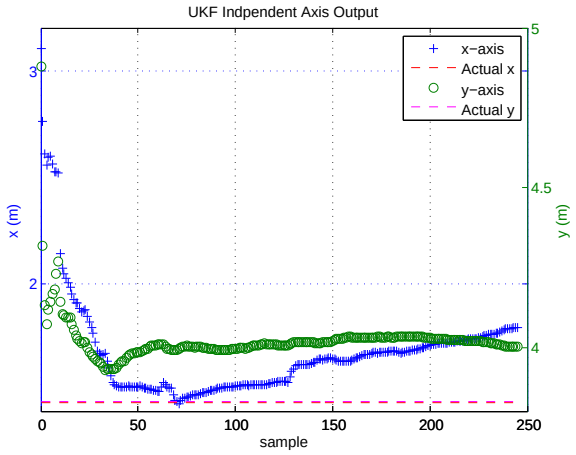

(a) Test 5 - Individual location axis output vs sample for UKF processing

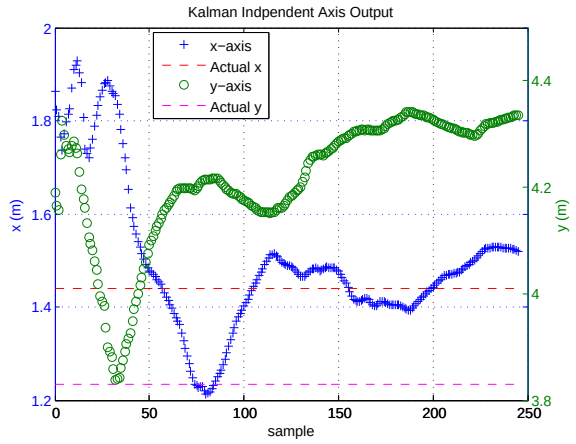

(b) Test 5 - Individual location axis output vs sample for KF processing

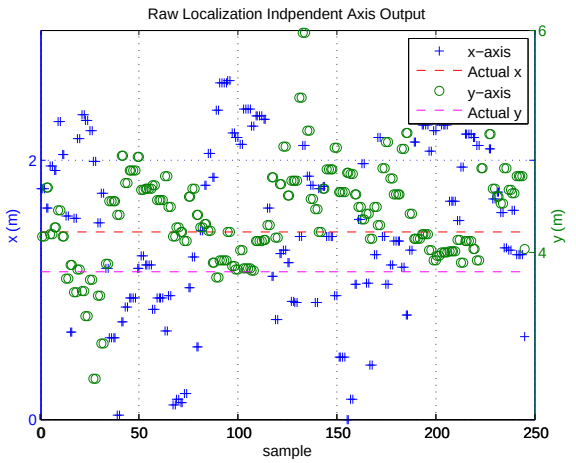

(c) Test 5 - Individual location axis output vs sample for raw localization data from the RTLS

Figure 4.10: Static Tag Test 5 - Test Site 2: Individual axis outputs of filters and RTLS system

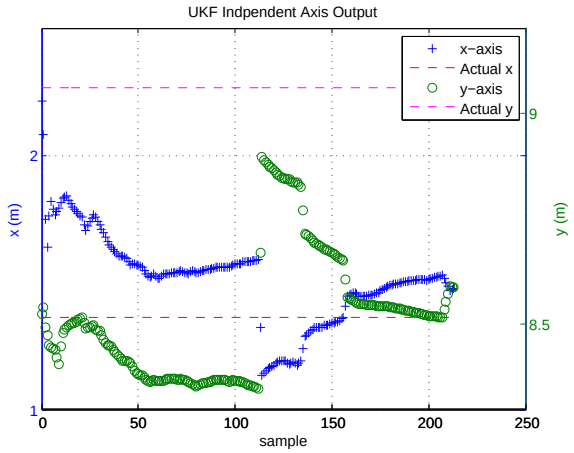

(a) Test 6 - Individual location axis output vs sample for UKF processing

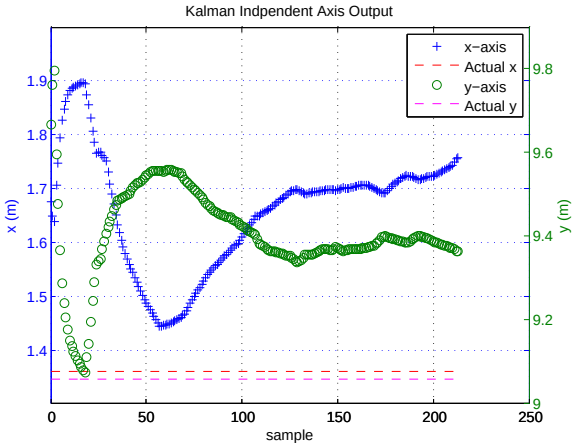

(b) Test 6 - Individual location axis output vs sample for KF processing

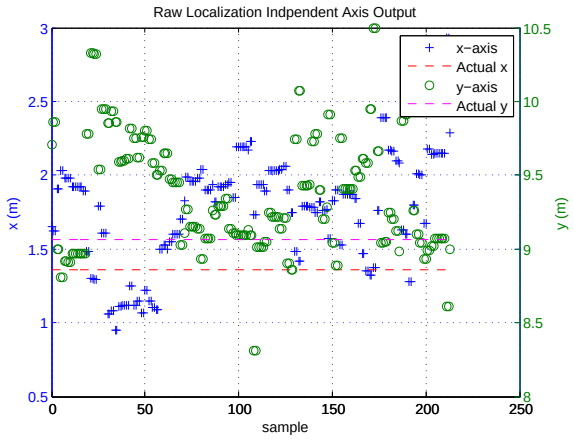

(c) Test 6 - Individual location axis output vs sample for raw localization data from the RTLS

Figure 4.11: Static Tag Test 6 - Test Site 2: Individual axis outputs of filters and RTLS system

Table 4.8: Test Site 2 - UKF anchor TOA distance measurement noise for static sample data sets

	R			
Test	Master	Slave 1	Slave 2	Slave 3
1	.2966	.0629	.3744	.0373
2	.1452	.0511	.0871	.0552
3	.1122	.0316	.0522	.0325
4	.0574	.0396	.2541	2.7970
5	.1198	18.8557	1.8699	.0462
6	.0447	4.7193	.1076	2.5742

$$\mathbf{P}_{t-1} = \begin{bmatrix} 10 & 10 & 1 \times 10^{-15} & 1 \times 10^{-15} & 1 \times 10^{-15} & 1 \times 10^{-15} \end{bmatrix}$$

The MSE and variance for each test and each coordinate axis was calculated and shown in Table 4.9 and 4.10 using (4.1) and (4.2). To allow for the initial adaptation period seen in Figure 4.3 for each filter, the first 10 estimation outputs of the UKF and KF were ignored and not used in their respective MSE and variance calculations. All samples were used for the raw data MSE and variance calculations.

Table 4.9: Test Site 2 - MSE for static sample data sets

		MSE		
Test	Axis	Raw Data	KF	UKF
1	x	.1054	.0213	.2392
	y	.2888	.1834	.0453
2	x	2.4548	2.3553	.4631
	y	.0359	.0232	.0130
3	x	.3330	.3786	.0916
	y	.1838	.1983	.0020
4	x	2.1051	2.1248	.4704
	y	24.0885	22.9851	.0326
5	x	.4495	.0248	.0551
	y	.4497	.1614	.0332
6	x	.2863	.0986	.0437
	y	.2430	.1280	.3141

Table 4.10: Test Site 2 - Variance for static sample data sets

		Variance - σ^2		
Test	Axis	Raw Data	KF	UKF
1	x	.0975	.0027	.0736
	y	.0326	.0038	.0220
2	x	.1669	.0051	.0250
	y	.0274	.0043	.0075
3	x	.0350	.0074	.0096
	y	.0253	.0004	.0019
4	x	.6419	.0094	.2363
	y	2.1448	.1644	.0095
5	x	.4452	.0230	.0167
	y	.1960	.0148	.0008
6	x	.1292	.0119	.0251
	y	.1517	.0098	.0232

3 Dynamic Testing - Site 1

To test a tag in motion, two data sets were collected with a single tag mounted on a wheeled tripod with an elevation of 1.08 m. Test 1 was conducted starting at $(-2.58, 0)$ and moved along the y axis to $(-2.58, 11.10)$. Test 2 was conducted with the tag starting at $(-6.47, 6.07)$ and moved along the x axis to $(0, -6.07)$. In both tests the tag was moved at a constant velocity of approximately 0.3 m/s. Filtering results are shown in Figure 4.12, 4.13, and 4.14.

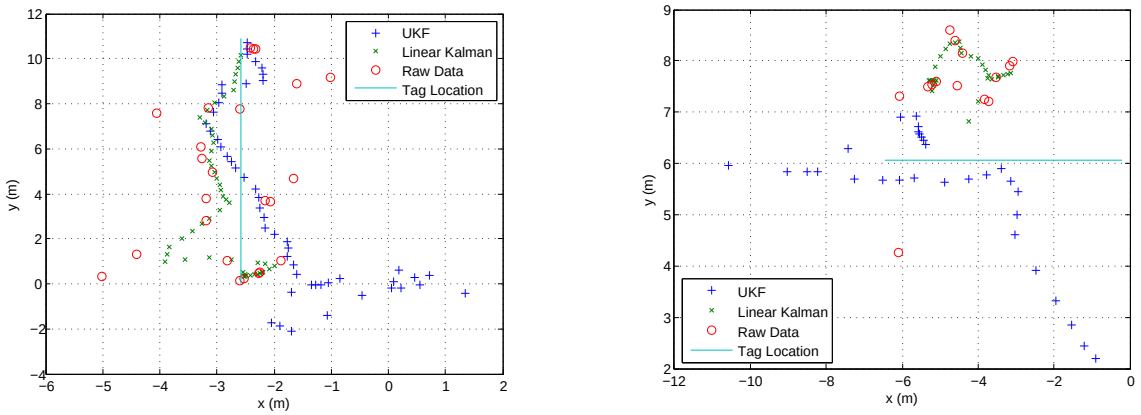

(a) Test 1

(b) Test 2

Figure 4.12: Dynamic Tag Tests- Test Site 1: Filtering results using sample data from the CSL RTLS

The measurement noise, R, could not be calculated from the data set in the manor that the static testing R was calculated. This is due to the fact that the tag is purposefully in motion, and thus its localization data will have a very large variance which is not representative of the measurement noise. Instead the R from static Test 1, Test Site 1, was used as a representative sample of the measurement noise of the system as shown in Table 4.2 and 4.3. The initial localization estimate was chosen as in the static testing but with velocity and acceleration of 0.5 m/s and 0 m/s as initial guesses. We choose initial covariances of 10 for the location and 1 for the velocity estimates, indicating low confidence in these estimates, and 1×10^{-9} for the acceleration estimate, indicating high confidence in this estimate. The resulting initial state and covariance estimates, $\bar{\theta}_{t-1}$ and $\mathbf{P}_{t-1}$, were then:

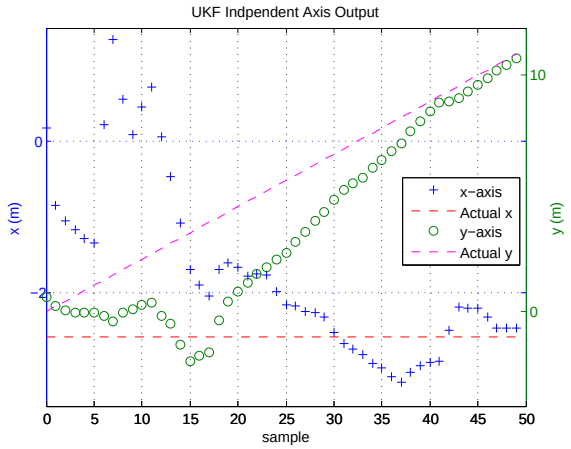

(a) Test 1 - Individual location axis output vs sample for UKF processing

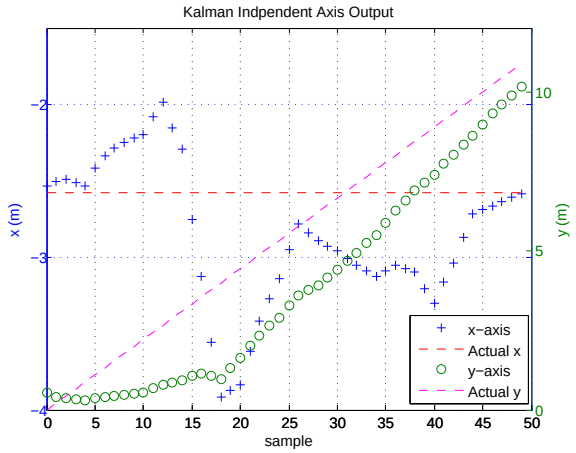

(b) Test 1 - Individual location axis output vs sample for KF processing

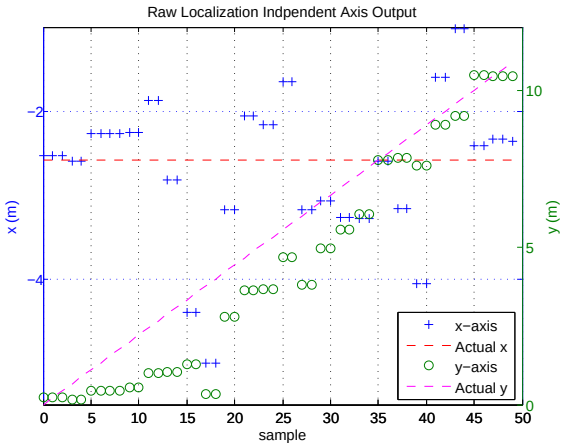

(c) Test 1 - Individual location axis output vs sample for raw localization data from the RTLS

Figure 4.13: Dynamic Tag Test 1 - Test Site 1: Individual axis outputs of filters and RTLS system

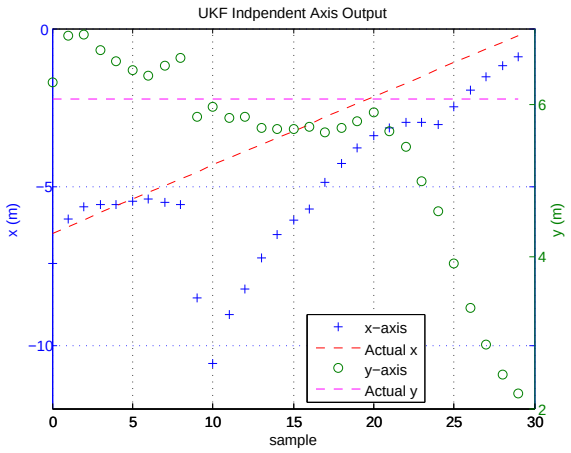

(a) Test 2 - Individual location axis output vs sample for UKF processing

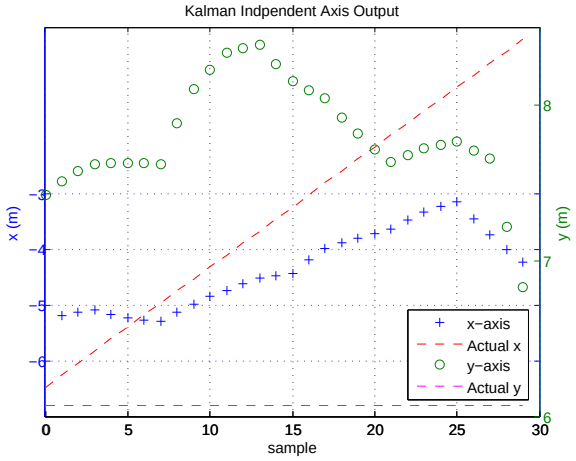

(b) Test 2 - Individual location axis output vs sample for KF processing

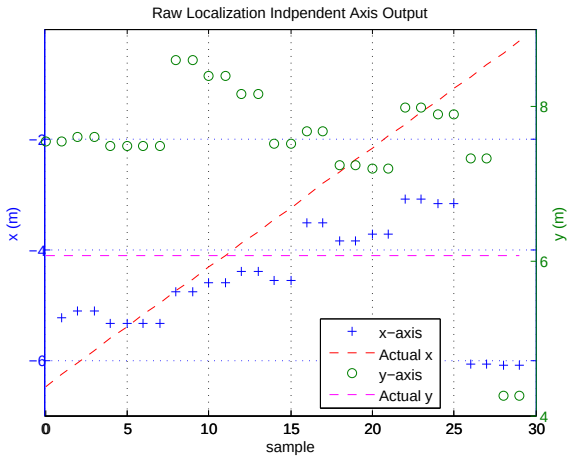

(c) Test 2 - Individual location axis output vs sample for raw localization data from the RTLS

Figure 4.14: Dynamic Tag Test 2 - Test Site 1: Individual axis outputs of filters and RTLS system

Table 4.11: Test Site 1 - Data range used in MSE and variance calculations

Test	Range (samples)
1	15−50
2	5−25

Table 4.12: Test Site 1 - MSE for dynamic sample data sets

		MSE		
Test	Axis	Raw Data	KF	UKF
1	y	1.0287	.3641	.3197
2	x	3.1225	3.5402	.2892

$$\bar{\theta}_{t-1} = \begin{bmatrix} -3.2 & 5.5 & 0.5 & 0.5 & 0 & 0 \end{bmatrix}$$

$$\mathbf{P}_{t-1} = \begin{bmatrix} 10 & 10 & 1 & 1 & 1 \times 10^{-9} & 1 \times 10^{-9} \end{bmatrix}$$

The MSE and variance for each test and each coordinate axis was calculated and shown in Table 4.12 and 4.13. As the tag was in motion, only the MSE and variance with respect to the axis of motion was computed as in (4.1) and (4.2). As we cannot know the exact location of the tag at any given sample, we compare the system output to an idealized linear path based on the start and end locations of the tag. To allow for the initial adaptation period and initial setup periods before and after the tag was in motion each test used only a subset of data points in the computation. These subsets are shown in Table 4.11 and were based on the range of the raw sample output where the tag appears to be in motion in 4.13c and 4.14c.

Table 4.13: Test Site 1 - Variance for dynamic sample data sets

		Variance - σ^2		
Test	Axis	Raw Data	KF	UKF
1	y	.9910	.1361	.2638
2	x	.2117	.0771	.2425

4 Dynamic Testing - Site 2

To test a tag in motion, two data sets were collected with a single tag mounted on a wheeled tripod with an elevation of 1.0 m. Test 1 was conducted starting at $(2.53, 0)$ and moved along the y axis to $(2.53, 13.57)$. Test 2 was conducted with the tag starting at $(0, 6.57)$ and moved along the x axis to $(7.45, 6.57)$. In both tests the tag was moved at a constant velocity of approximately 0.3 m/s. Filtering results are shown in Figure 4.15, 4.16, and 4.17.

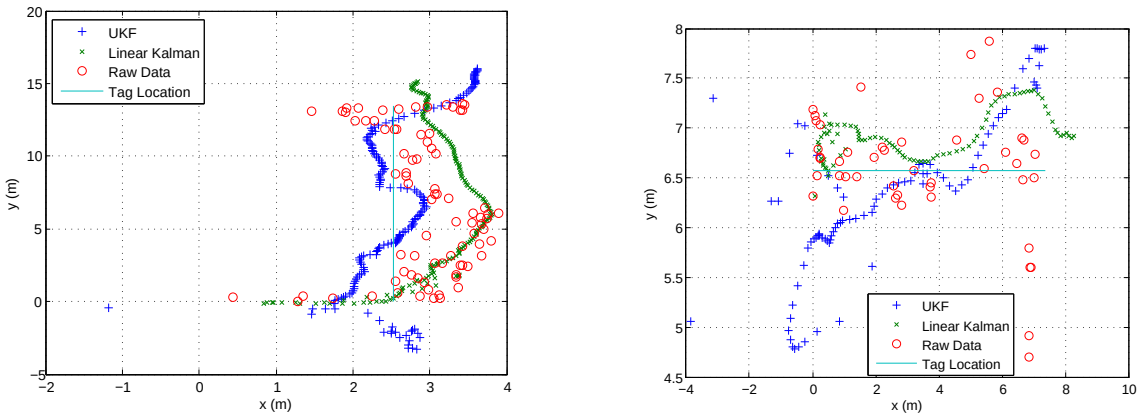

(a) Test 1 (b) Test 2

Figure 4.15: Dynamic Tag Tests- Test Site 2: Filtering results using sample data from the CSL RTLS

The measurement noise, R, could not be calculated from the data set in the manor that the static testing R was calculated. This is due to the fact that the tag is purposefully in motion, and thus its localization data will have a very large variance which is not representative of the measurement noise. Instead the R from static Test 1, Test Site 2, was used as a representative sample of the measurement noise of the system as shown in Table 4.7 and 4.8.

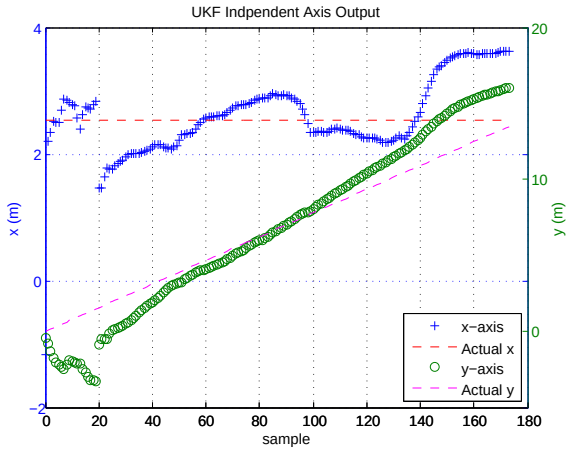

(a) Test 1 - Individual location axis output vs sample for UKF processing

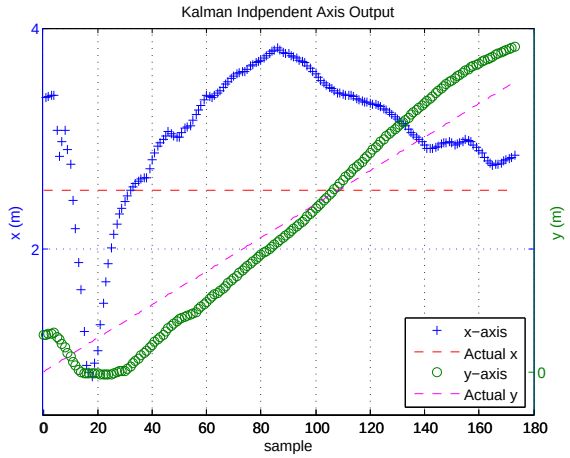

(b) Test 1 - Individual location axis output vs sample for KF processing

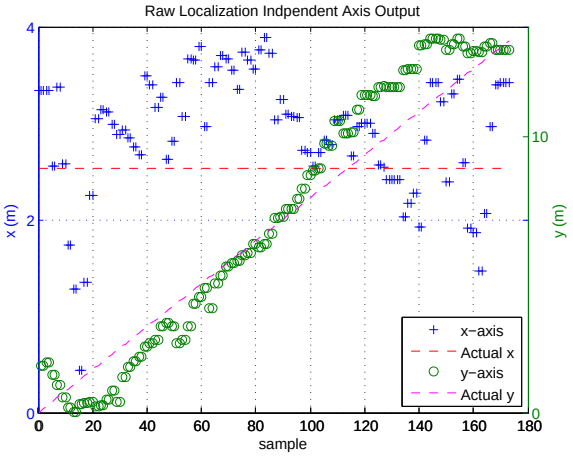

(c) Test 1 - Individual location axis output vs sample for raw localization data from the RTLS

Figure 4.16: Dynamic Tag Test 1 - Test Site 2: Individual axis outputs of filters and RTLS system

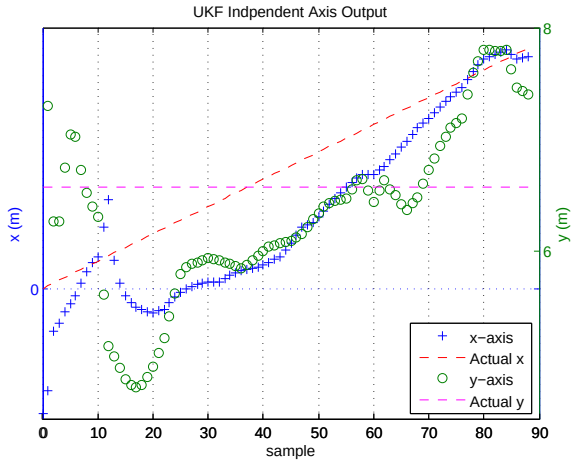

(a) Test 2 - Individual location axis output vs sample for UKF processing

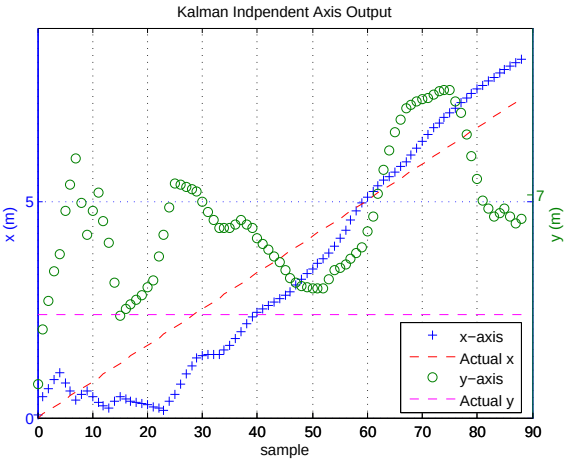

(b) Test 2 - Individual location axis output vs sample for KF processing

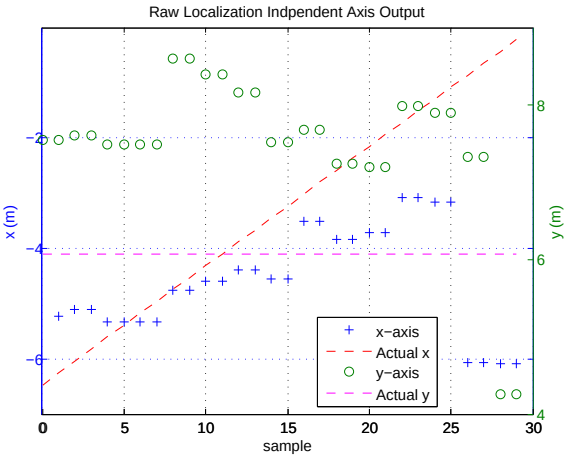

(c) Test 2 - Individual location axis output vs sample for raw localization data from the RTLS

Figure 4.17: Dynamic Tag Test 2 - Test Site 2: Individual axis outputs of filters and RTLS system

Table 4.14: Test Site 2 - Data range used in MSE and variance calculations

Test	Range (samples)
1	20−140
2	20−80

Table 4.15: Test Site 2 - MSE for dynamic sample data sets

		MSE		
Test	Axis	Raw Data	KF	UKF
1	y	.4749	.7361	.1360
2	x	.3173	.0566	.5801

The initial localization estimate was chosen as in the static testing but with velocity and acceleration of 0.5 m/s and 0 m/s as initial guesses. We choose initial covariances of 10 for the location and and 1 velocity estimates, indicating low confidence in these estimates, and 1×10^{-9} for the acceleration estimate, indicating high confidence in this estimate. The resulting initial state and covariance estimates, $\bar{\theta}_{t-1}$ and $\mathbf{P}_{t-1}$, were then:

$$\bar{\theta}_{t-1} = \begin{bmatrix} 3.72 & 6.78 & 0.5 & 0.5 & 0 & 0 \end{bmatrix}$$

$$\mathbf{P}_{t-1} = \begin{bmatrix} 10 & 10 & 1 & 1 & 1\times10^{-9} & 1\times10^{-9} \end{bmatrix}$$

The MSE and variance for each test and each coordinate axis was calculated and shown in Table 4.15 and 4.16. As the tag was in motion, only the MSE and variance with respect to the axis of motion was computed as in (4.1) and (4.2). As we cannot know the exact location of the tag at any given sample, we compare the system output to an idealized linear path based on the start and end locations of the tag. To allow for the initial adaptation period and initial setup periods before and after the tag was in motion each test used only a subset of data points in the computation. These subsets are shown in Table 4.14 and were based on the range of the raw sample output where the tag appears to be in motion in 4.16c and 4.17c.

Table 4.16: Test Site 2 - Variance for dynamic sample data sets

		Variance - σ^2		
Test	Axis	Raw Data	KF	UKF
1	y	.2045	.3248	.1159
2	x	.3038	.0306	.1144

Chapter 5

Analysis

1 Static Testing

In the static testing at Test Site 1 the UKF and KF were found to reduce the variance of the static localization estimate compared to the raw output of the RTLS. In these data sets the UKF showed a lower variance, but a higher MSE than the raw output, while the KF showed both lower MSE and variance. This pattern held for both static sample sets. The variance of the KF was also found to be lower than the UKF. Both algorithms produced lower variance and thus a more precise localization output, with the KF being more accurate. The total MSE and variance for all static tests at Site 1 is shown in Figure 5.1 and 5.2. The total MSE and variance was computed by summing the MSE and variance from each test for each output source.

In the static testing at Test Site 2 the UKF and KF were found to reduce the variance and MSE of the static localization estimate compared to the raw output of the RTLS. In all but Test 1 x-axis, and Test 6 y-axis, the UKF produced a localization output MSE up to 3 orders of magnitude smaller than the raw data output. The UKF also showed lower variance on all tests up to 2 magnitudes smaller than the raw output. The total MSE and variance for all static tests at Site 1 is shown in Figure 5.3 and 5.4.

The KF at Test Site 2 also reduced the MSE and variance of the output data up to 2 magnitudes, though it tracked the raw data output more closely than the UKF. This can be seen clearly in Test 2 and 4 in Figure 4.5b and 4.5d. In these test the raw data output had a large MSE in one or both of the axis as seen in Table 4.9. The results show the KF reduced the MSE and variance of the output data, but showed a much larger MSE than

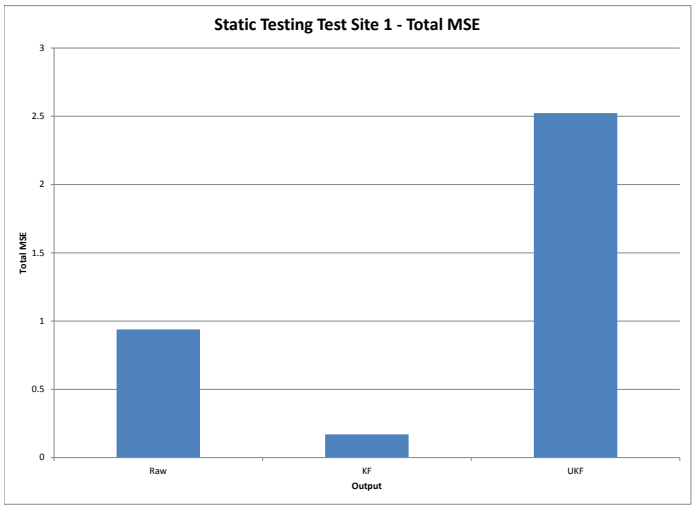

Figure 5.1: Static Testing - Site 1: Total MSE for each output source. The KF shows a 81.9% reduction and the UKF a 168.65% increase in MSE vs. the raw output.

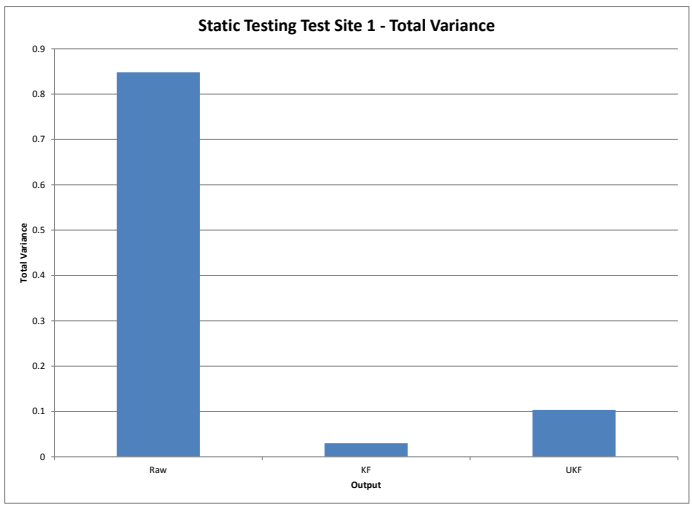

Figure 5.2: Static Testing - Site 1: Total variance for each output source. The KF shows a 96.46% and the UKF a 87.81% reduction in variance vs. the raw output.

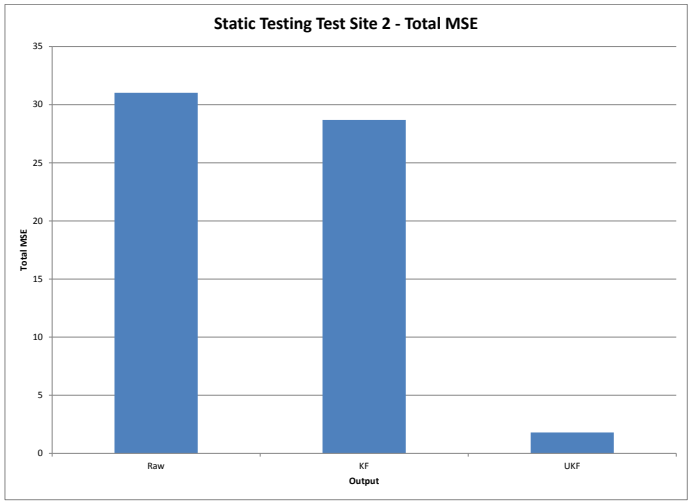

Figure 5.3: Static Testing - Site 2: Total MSE for each output source. The KF shows a 7.55% and the UKF a 94.19% reduction in MSE vs. the raw output.

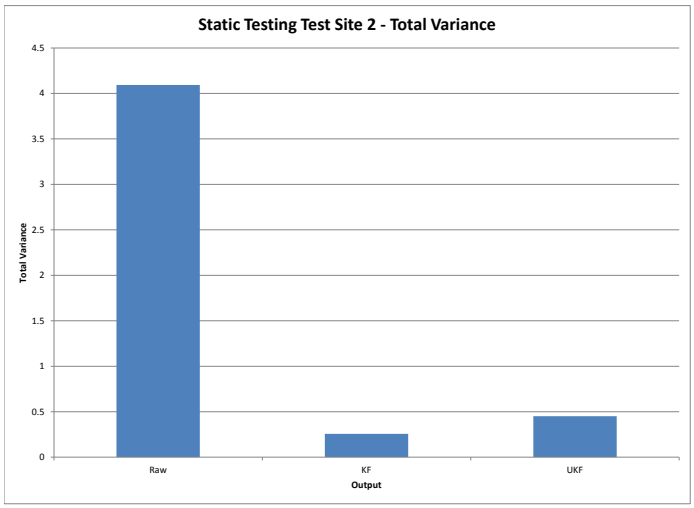

Figure 5.4: Static Testing - Site 2: Total variance for each output source. The KF shows a 93.72% and the UKF a 88.98% reduction in variance vs. the raw output.

the UKF. This is because the KF was filtering the final localization output, and thus could only track the raw output, instead of the actual tag position based on the TOA distance measurements as the UKF did.

The UKF filters the raw TOA distance measurements of the RTLS. This removes any coupling between the trilateration algorithms and thus the localization output of the RTLS software and the algorithm's localization estimate. This can be seen in all test cases from Test Site 2 where the UKF output is clearly separate from the raw localization and KF output. In many cases the KF seems to more or less smooth the static data set, where the UKF computes a distinct localization output. This appears to be an advantage of the UKF and TOA distance data set, especially when the raw output has high MSE or variance.

It can also be seen, particularly in Test Site 1 Figure 4.1, that the UKF clustering appears to be offset from the actual tag location in some instances. This gives it a higher MSE than than the raw data and KF despite its low variance. The lower MSE of the raw and KF data could indicate some sort of offset correction was being employed by the RTLS system to correct for an internal or hardware bias we are unaware of and the UKF is not taking into account. The higher MSE of the UKF in these instances could also be due to inherent linearalization errors present in the unscented transformation.

The outliers seen in the UKF and KF, particularly in Figure 4.1a, can be attributed to the algorithm's adaptation period. This adaptation period is clearly seen in the independent axis outputs, such as Figure 4.2a, where the first 28 samples show high variance and an eruption before reaching a stable output. Similar initial adaptation periods can also be seen for the KF and UKF in Figure 4.3, 4.2, and Figure 4.6-4.11, where the first 10-15 samples show a adaptation curve before reaching a relatively stable output.

These adaptation periods occur because of our initial estimation of the $\bar{\theta}$ and $\mathbf{P}$ matrices used by the KF and UKF algorithms. Our initial estimate of the tag position at the center of the tracking area with low confidence, and zero velocity and acceleration with high confidence, was a un-biased starting point, but was not the true initial state of the system. As it is highly unlikely the exact state of the system would be known in real-world conditions, or even could be known in testing based on the available data, our initial estimate is appropriate. The KF and UKF use these initial estimates, but recursively correct

themselves as the data set is processed. This results in the adaptation period seen, and the subsequent initial outliers. If the exact state of the system had been used as the initial estimate, these adaptation periods would not be seen.

2 Dynamic Testing

The results from the dynamic testing show a similar trend as the static testing, but may not be compared in the same manor. In the dynamic testing, the computation of a full MSE and variance are not possible as the tag is in motion, and its exact location at each data sample cannot be known based on our setup. The system samples the tag once per second in a time division multiplexed algorithm, but the exact time of each sample is not known by the user. Thus we cannot know the exact position of the tag at any given point in time.

To complicate matters further the sample data from these tests also includes data points at the beginning and end of the test where the tag was static before and after movement. These data points, technically outside the tracking area, were still captured by the system and processed. This resulted in the outlier points seen in Figure 4.12 and 4.15 in both the KF and UKF at the beginning and end of the dynamic tests. The system output is unreliable at the edge of and outside the contained tracking area, thus the algorithm output at these points becomes divergent and should be disregarded.

To account for these issues, yet still attempt to quantify the system performance, the MSE and variance for the dynamic tests was computed only along the axis perpendicular to the tag motion, and using only a subset of the data in which the tag was known to be in motion. The MSE was calculated using an ideal linear motion estimate based on the known start and end locations of the tag. The off-axis location reading was compared against this linear ideal to compute the resulting MSE. This method is not perfect, as it quantifies the performance of only one axis, but it does provide a means to compare the dynamic performance of the system.

The dynamic testing at Site 1 shows the UKF produced a lower MSE and variance than the raw localization data in all tests except Test 2, y-axis, where it showed a slightly higher

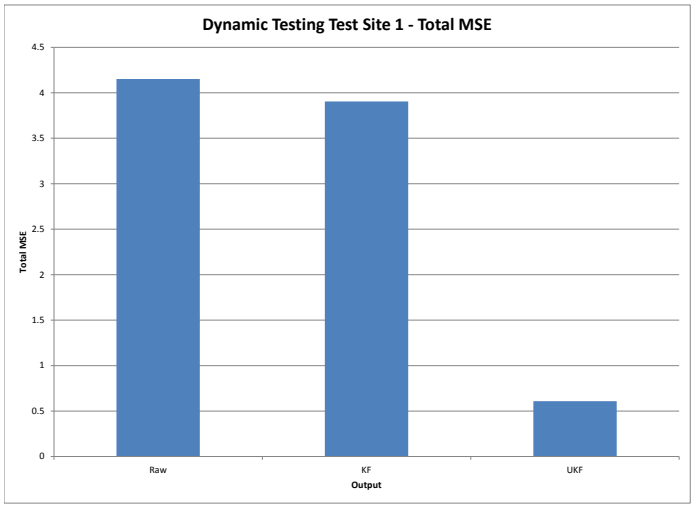

Figure 5.5: Dynamic Testing - Site 1: Total MSE for each output source. The KF shows a 5.95% and the UKF a 85.32% reduction in MSE vs. the raw output.

variance. The KF also showed a lower MSE and variance than the raw data, except in Test 2, y-axis, where it showed a higher MSE. The total MSE and variance for all dynamic tests at Site 1 is shown in Figure 5.5 and 5.6.

The data from Site 1 Test 2, however; can be seen to be almost unusable as localization data based on the output seen in Figure 4.12. The raw output and filter outputs do exhibit some movement along the tag path, but it is very limited and confined to the first half of the path. The lack of quality of the localization data for this test can be explained by the shortness of the path. In this test the tag moves only 6 m which is only 2 m greater than the rated accuracy of the system. The movement of the tag is lost within the given inaccuracy of the system and thus the tag path is not captured by the sample data.

The dynamic testing at Site 2 shows the UKF produced a lower MSE and variance than the raw localization data in all tests except Test 1, y-axis, where it showed a slightly higher MSE. The KF showed mixed results, with a lower MSE and variance than the raw data in Test 2, but higher in Test 1. The KF outperformed the UKF in Test 2, but the UKF outperformed the KF in Test 1. Again, here the data from Test 2 is more difficult to analyze as the tag traveled a shorter distance than in Test 1, in this case 7.45 m. The total MSE and variance for all dynamic tests at Site 1 is shown in Figure 5.7 and 5.8.

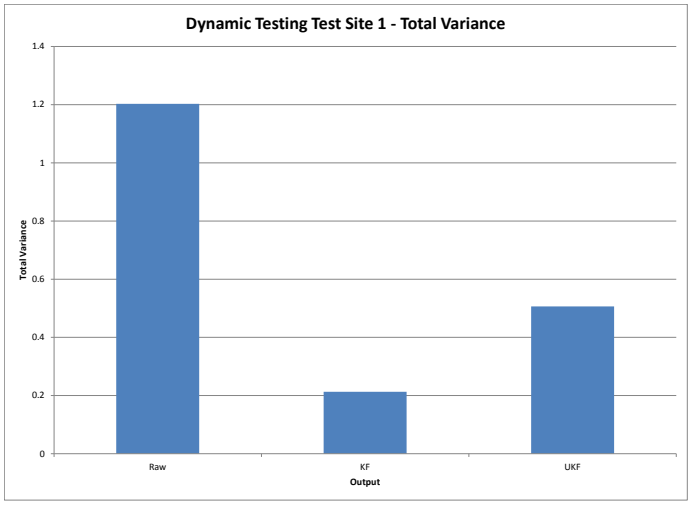

Figure 5.6: Dynamic Testing - Site 1: Total variance for each output source. The KF shows a 82.27% and the UKF an 57.90% reduction in variance vs. the raw output.

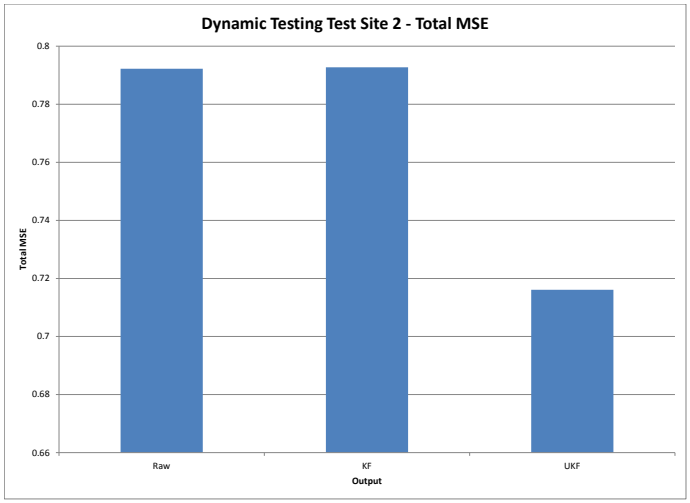

Figure 5.7: Dynamic Testing - Site 2: Total MSE for each output source. The KF shows a 0.06% increase and the UKF an 9.61% reduction in MSE vs. the raw output.

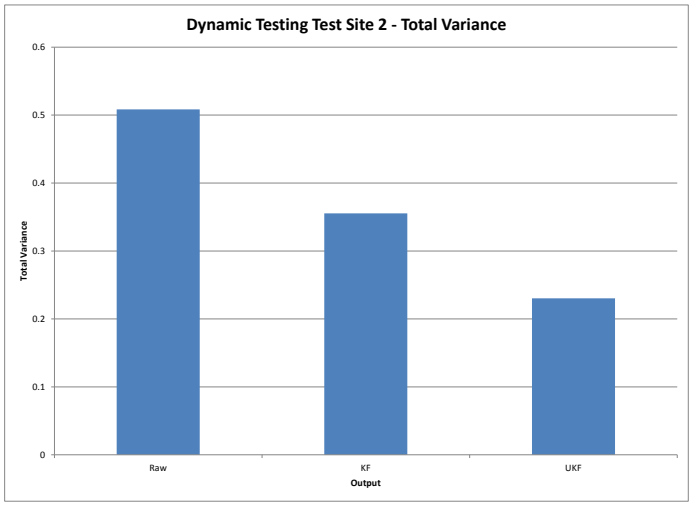

Figure 5.8: Dynamic Testing - Site 2: Total variance for each output source. The KF shows a 30.01% and the UKF an 54.69% reduction in variance vs. the raw output.

3 Overall Analysis

Based on the dynamic and static testing at both test sites, it can be seen that both the UKF and KF reduce the variance and MSE of the raw localization output. Table 5.1 shows the overall MSE and variance reduction versus the raw output for each filter method. This was computed by taking the average of the total MSE and variance readings from all tests, all axis, and computing the percent vs. the raw output.

From Table 5.1 and the individual static and dynamic comparison figures it can be seen that the data shows the KF produces an overall lower MSE and variance than the UKF, however; this must be viewed with an important caveat applied. The UKF generally produces a more accurate localization output than the KF in scenarios where the raw RTLS output has a high MSE or variance. The KF generally produces a more accurate localization output than the UKF when the raw output has a relatively low MSE or variance. The KF

Table 5.1: Overall MSE and variance percent reduction of filtering algorithm output vs. raw RTLS localization output

	KF (%)	UKF (%)
MSE	23.83	5.12
σ^2	75.63	72.34

appears to act mainly as a smoother of the raw data output, while the UKF uses the TAO distance measurements directly, decoupling the localization from the RTLS trilateration routine. This allows the UKF to break away from the raw output to produce a independent localization result in scenarios of high noise.

As we have no visibility into the RTLS system, or its internal localization algorithms, we cannot draw conclusions as to the relation between the raw output and the UKF output in terms of accuracy. Obviously the UKF improves localization performance, but how much of that improvement is based on the algorithm, and what may be attributed to errors or computational differences in the RTLS system cannot be said. The RTLS system appears to show a high discontinuity in some tests where the TOA distance measurements don't seem to correlate properly with the final localization output. This can be seen in the tests where the raw output and KF has high MSE and the UKF produces a much lower MSE output such as Static Test 4 from Test Site 2 in Figure 4.5d, and Static Test 2 from Test Site 1 in Figure 4.1b.

The accuracy and performance of the KF and UKF also rely heavily on the values used for the initial state and covariance estimates, and the process and measurement noise. These values were chosen both empirically and based on the given variance of the input data, but can be manipulated to tune the filter performance to a given environment and task. It was found that a different set of initial estimates works better for static and dynamic tag behavior based on the known conditions of the testing.

Selection of the measurement noise variance for the UKF filtering was found to perform best when the computed variance of the TOA distance reading from each tag/anchor pair was used based on the anchors being used for that particular localization sample. This prevented tag/anchor pair TOA distance readings which displayed a high variance, possibly due to multi-path or local noise interference, from influencing localization computations performed with lower variance tag/anchor data. This TOA distance variance variance is seen in Table 4.8 from Test Site 2, where the variance among the anchors in Test 3 and 4 vary by up to 3 orders of magnitude.

Chapter 6

Conclusion

In this paper Kalman filtering techniques were applied to the output of a commercial real-time RFID localization system to reduce noise and improve localization accuracy and precision. The RFID RTLS system was set up in two indoor environments and a single tag tracked using both static and dynamic tracking scenarios. The environments were chosen to simulate two common noisy work environments with interference from various RF sources and non-line of sight situations. System models for the KF and UKF were developed and applied to the TOA distance and raw localization output of the RTLS system. The filtering algorithms were tuned to the environments and known system characteristics using the variance of the sample data sets and knowledge of the testing scenarios.

Results show the KF and UKF reduced the MSE and variance of the raw output data by up to 25% and 75% respectively overall. The KF was found to outperform the UKF in testing scenarios where the raw localization output had relatively low MSE and variance, producing final localization results with lower MSE and variance than the UKF. The UKF, however; was found to outperform the KF in scenarios where the raw localization output had high relative MSE and variance. In these scenarios the UKF was able to use the TOA distance sample data instead of the raw localization output to produce a more accurate result than the KF which used only the raw localization output.

The determination of the measurement noise variance was found to be successfully computed as the variance of the sample data set for either the raw localization output for the KF, or the variance of the anchor/tag pair TOA distance readings for the UKF. From the 4 TOA distance variances calculated for the UKF, utilizing a dynamic measurement noise matrix which updated the variance used in each recursion of the UKF algorithm based on

the anchors chosen for that sample was found to produce optimal results. The selection of the sample data for UKF processing based on the two anchor/tag pairs with the highest uplink RSSI value was found to produce optimal results when coupled with the dynamic measurement noise variance.

Overall it was found the application of the KF or UKF to the raw output of the CSL RTLS system reduced the noise and improved the localization accuracy and precision of the system. The data processing was performed in Matlab after the data was collected, and could easily be integrated into a common post-processing solution. In our setup the data was computed in batch after all samples had been collected, but the same methods could be applied to process the data on a sample by sample basis in real-time.

1 Future Work

Further testing of dynamic tag movement, including scenarios with non-linear paths, would help to develop a stronger basis for the performance of the system when tracking moving tags. This could also be incorporated with testing of transitions from static to dynamic movement to develop an algorithm to dynamically adjust the filter parameters based on the observed tag state.

The RTLS system appears to show a high discontinuity in some tests where the TOA distance measurements don't seem to correlate properly with the final localization output. This can be seen in the tests where the raw output and KF has high MSE and the UKF produces a much lower MSE output. An investigation into the computational methods of the RTLS and its determination of trilateration data could help resolve this incongruity.

To extend this work beyond Kalman filters, investigation into other filtering techniques, such as adaptive filers and particle filtering, could be performed and compared against the results presented in this research. Other methods may provide better noise reduction or improve the dynamic tracking. Adaptive filtering approaches could also increase the flexibility and ease of implementation of the system as the initial state of the tracking environment and system noise characteristics would not have to be pre-computed as is needed when using Kalman filtering techniques.

Bibliography

[1] M. Harris, "The way through the flames," *Spectrum, IEEE*, vol. 50, no. 9, pp. 30–35, September 2013.

[2] A. Akanmu, S. Rasheed, and I. Qader, *Spatial Mapping Approach to Component Tracking Using RTLS System.* [Online]. Available: http://ascelibrary.org/doi/abs/10.1061/9780784412909.035

[3] T. Sanpechuda and L. Kovavisaruch, "A review of rfid localization: Applications and techniques," in *Electrical Engineering/Electronics, Computer, Telecommunications and Information Technology, 2008. ECTI-CON 2008. 5th International Conference on*, vol. 2, 2008, pp. 769–772.

[4] S.-Y. Lee and J.-T. Park, "Nlos error mitigation in a location estimation of object based on rtls using kalman filter," in *SICE-ICASE, 2006. International Joint Conference*, oct. 2006, pp. 2942 –2946.

[5] A. Bekkali, H. Sanson, and M. Matsumoto, "Rfid indoor positioning based on probabilistic rfid map and kalman filtering," in *Wireless and Mobile Computing, Networking and Communications, 2007. WiMOB 2007. Third IEEE International Conference on*, oct. 2007, p. 21.

[6] C. S. Limited, *CSL Real-Time Localization System - User's Manual*, 3rd ed.

[7] L. Peneda, A. Azenha, and A. Carvalho, "Trilateration for indoors positioning within the framework of wireless communications," in *Industrial Electronics, 2009. IECON '09. 35th Annual Conference of IEEE*, Nov 2009, pp. 2732–2737.

[8] T. Nick, J. Goetze, W. John, and G. Stoenner, "Comparison of extended and unscented kalman filter for localization of passive uhf rfid labels," in *General Assembly and Scientific Symposium, 2011 XXXth URSI*, aug. 2011, pp. 1 –4.

[9] T. Nick, J. Gotze, W. John, and G. Stoenner, "Localization of uhf rfid labels with reference tags and unscented kalman filter," in *RFID-Technologies and Applications (RFID-TA), 2011 IEEE International Conference on*, sept. 2011, pp. 168 –173.

[10] P. H. Abreu, J. Xavier, D. C. Silva, L. P. Reis, and M. Petry, "Using kalman filters to reduce noise from rfid location system," *The Scientific World Journal*, 2014.

[11] S.-I. Ko, J.-S. Choi, and B. hoon Kim, "Performance enhancement of indoor mobile localization system using unscented kalman filter," in *SICE-ICASE, 2006. International Joint Conference*, 2006, pp. 1355–1360.

[12] A. Paul and E. Wan, "Wi-fi based indoor localization and tracking using sigma-point kalman filtering methods," in *Position, Location and Navigation Symposium, 2008 IEEE/ION*, may 2008, pp. 646 –659.

[13] F. Martinelli, "Robot localization: comparable performance of ekf and ukf in some interesting indoor settings," in *Control and Automation, 2008 16th Mediterranean Conference on*, june 2008, pp. 499 –504.

[14] T. Bo, C. Pingyuan, and C. Yangzhou, "Sigma-point kalman filters for gps based position estimation," in *Information, Communications and Signal Processing, 2005 Fifth International Conference on*, 0-0 2005, pp. 213 –217.

[15] R. Van Der Merwe and E. A. Wan, "Sigma-point kalman filters for integrated navigation," in *Proceedings of the 60th Annual Meeting of the Institute of Navigation (ION)*, 2004, pp. 641–654.

[16] F. Daum, "Nonlinear filters: beyond the kalman filter," *Aerospace and Electronic Systems Magazine, IEEE*, vol. 20, no. 8, pp. 57 –69, aug. 2005.

[17] E. Wan, "Sigma-point filters: An overview with applications to integrated navigation and vision assisted control," in *Nonlinear Statistical Signal Processing Workshop, 2006 IEEE*, 2006, pp. 201–202.

[18] S. J. Julier and J. K. Uhlmann, "New extension of the kalman filter to nonlinear systems," in *AeroSense'97*. International Society for Optics and Photonics, 1997, pp. 182–193.

[19] A. Paul and E. Wan, "Rssi-based indoor localization and tracking using sigma-point kalman smoothers," *Selected Topics in Signal Processing, IEEE Journal of*, vol. 3, no. 5, pp. 860 –873, oct. 2009.

[20] J. Crassidis, "Sigma-point kalman filtering for integrated gps and inertial navigation," *Aerospace and Electronic Systems, IEEE Transactions on*, vol. 42, no. 2, pp. 750 – 756, april 2006.

[21] J. Hartikainen, A. Solin, and S. Srkk. (2011, August) Ekf/ukf toolbox for matlab v1.3. Matlab Library. Department of Biomedical Engineering and Computational Science, Aalto University School of Science. P.O.Box 1100, FI-00076 AALTO, Espoo, Finland. [Online]. Available: http://becs.aalto.fi/en/research/bayes/ekfukf/